gation products are 12 nt for segments 1, 3, and 7, 13 nt for segments 5 and 8, 14 nt for segment 6, 18 nt for segment 4, and 19 nt for segment 2. Since we detected comparable amounts of each RNA product in the absence or presence of exogenous NP (Fig. 1E), it is concluded that NP, like MCM, does not stimulate the initiation reaction (9). Thus, NP may be required for a step(s) after the initiation and the early elongation steps, in which short cRNAs are synthesized.

To examine whether NP stimulates the transition of the viral polymerase from initiation to elongation, that is, the promoter escape of the viral polymerase, unprimed limited elongation assays were first performed in the absence of UTP, and elongation reactions were restarted by the addition of UTP (Fig. 1F). MCM (0.5 pmol) or exogenous NP (3 pmol) was also added either before or after the limited elongation. The full-length cRNA was synthesized by restarting the limited elongation reaction performed in the presence of MCM (lane 2) or exogenous NP (lane 4) during the limited elongation reaction. Thus, it is quite likely that, to avoid abortive RNA synthesis by the viral polymerase, MCM and NP are required for the viral polymerase prior to its movement along a 12- to 19-nt-long vRNA template from the 3′ terminus of vRNA, where the hairpin loop and double-stranded promoter region are located. Since the initiation reaction was not stimulated by NP (Fig. 1E) and since the viral polymerase could not transit from initiation to elongation in the absence of NP (Fig. 1F), it is possible that NP stimulates elongation complexes during the promoter escape of the viral polymerase, as does MCM (9). A cell-free virus genome replication reaction was also carried out (Fig. 1G) in the presence of MCM (lane 2; 0.5 pmol) or NP (lane 3; 3 pmol) with a low concentration of UTP to slow down the reaction and synthesize a ladder of nascent cRNA chains in order to examine the length of elongated nascent cRNA chains. We found that comparable amounts of cRNA with a shorter length (~100 nt) are synthesized in the presence of either MCM or NP. In contrast, the amount of longer cRNAs (>100 nt) stimulated by MCM was greater than that stimulated by NP (Fig. 1G, compare lane 2 with lane 3). Therefore, it is quite likely that MCM promotes the elongation process more effectively than NP, possibly due to the weak interaction of exogenously added NP with long nascent cRNA, as described later. Taking these results together, it is strongly suggested that NP, like MCM, stimulates the promoter escape of the viral polymerase. Previous reports showed that the target of MCM is PA (9), whereas that of NP is PB1 and PB2 (1). Therefore, it is possible that the replication stimulation mechanisms of NP and MCM are distinct from each other.

Encapsidation of newly synthesized virus genome by NP. Previously, we proposed that MCM stimulates virus genome replication by acting as a scaffold between nascent cRNA chains and the viral polymerase during the promoter escape of the polymerase (9). Since NP has both RNA and viral polymerase binding activities, it should be speculated that NP, like MCM, also functions as a scaffold between newly synthesized RNA and the viral polymerase. To address this, we tried to pull down the replicated cRNA chains associated with His-tagged MCM or NP using Ni-nitrilotriacetic acid (NTA) resin (Fig. 2A). The cell-free virus genome replication reaction was carried out in the presence of an equal molar amount of MCM (lanes 1 and 3) or NP (lanes 2 and 4) with a low concentration

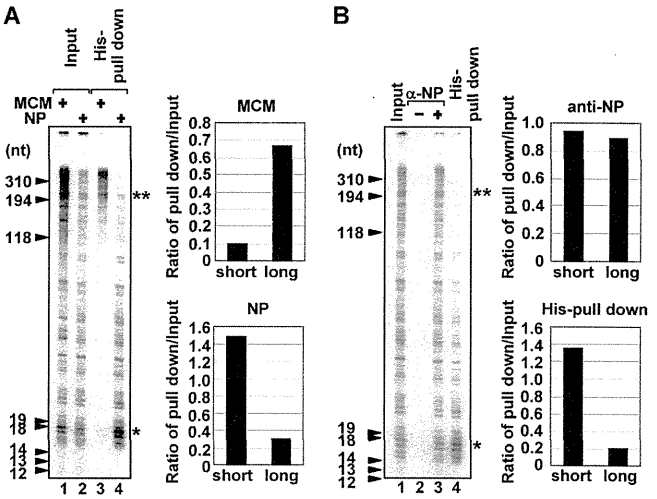

FIG. 2. Encapsidation of nascent cRNA with NP. (A) *De novo* RNA synthesis was carried out in the presence of His-MCM (lanes 1 and 3; 20 pmol) or His-NP (lanes 2 and 4; 20 pmol) with 0.3 μM UTP and 250 μM each ATP, CTP, and GTP and 10 μCi of [α-^{32}P]UTP (3,000 Ci/mmol) in a final volume of 200 μl. The products were purified with His-MCM (lane 3) or His-NP (lane 4) by using Ni-NTA resin. Lanes 1 and 2 represent 20% of the input amounts. The band intensities of short (*) and long (**) nascent cRNA products were quantitatively measured with ImageJ software, and the relative intensity of newly synthesized cRNA coprecipitated with MCM or NP against the input fraction is indicated. (B) *De novo* RNA synthesis was carried out with the authentic vRNP in the presence of His-NP as described for panel A. The newly synthesized RNA products were coimmunoprecipitated without (lane 2) or with (lane 3) anti-NP antibody. Lane 1 shows 20% of the input amount. The product purified by Ni-NTA resin is also represented in lane 4. The band intensities of short (*) and long (**) nascent cRNA products were quantitatively measured with ImageJ software, and the relative intensity of newly synthesized cRNA precipitated by using anti-NP antibody or Ni-NTA resin against input fraction is indicated. α, anti.

of UTP in order to examine the length of copurified RNA as shown in Fig. 1G. As shown in input lanes, MCM stimulated the elongation process more effectively than NP (Fig. 1E and 2A, lanes 1 and 2). Further, longer nascent cRNA chains were preferentially copurified with MCM (Fig. 2A, lane 3), suggesting that MCM stabilizes the elongation complex and thereby makes the viral polymerase escape the promoter successfully. It also seems likely that MCM has a role in the elongation process, but its precise mechanism is still unknown. In contrast, rather shorter cRNA chains were associated with exogenous NP (lane 4). After or along with virus genome replication, the newly synthesized virus genome has to be encapsidated by exogenous NP to form RNP complexes as templates for the next phase of virus genome replication and to protect the virus genome from degradation by cellular nucleases (33). It is hypothesized that encapsidation proceeds by targeting exogenous NP to the nascent RNA through the interaction between NP and the viral polymerase bound to the 5′ end of the nascent RNA to allow NP to interact with the viral RNA preferentially with respect to other cellular RNA species (1, 8, 11, 22), and then subsequently NP is recruited through NP-NP oligomerization (3, 23). In our cell-free system, we found that exogenous NP interacts with shorter cRNA (Fig. 2A, lane 4) without the addition of soluble viral polymerases, which could bind to

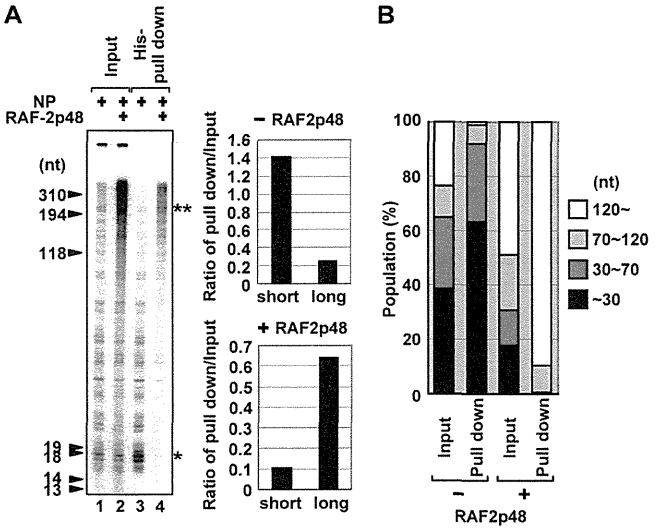

FIG. 3. The stimulatory activity of RAF-2p48/UAP56 in encapsidation of nascent cRNA. (A) RNA synthesis was performed in the absence (lanes 1 and 3) or presence (lanes 2 and 4) of recombinant RAF-2p48/UAP56 with His-NP as described in the legend of Fig. 2. The products were purified with His-NP by using Ni-NTA resin (lanes 3 and 4). Twenty percent of the input amounts is shown in lanes 1 and 2. The band intensities of short (*) and long (**) nascent cRNA products were quantitatively measured with ImageJ software, and the relative intensity of cRNA coprecipitated with NP in the absence or presence of RAF-2p48 against input fraction is indicated. (B) The band intensities of the regions corresponding to RNAs of less than 30 nt, 30 to 70 nt, 70 to 120 nt, and more than 120 nt in each lane in panel A were quantitatively measured with ImageJ software, and the results are indicated as a percentage of the total intensity of each lane.

the 5′ end of the nascent RNA and be a target of NP. It might be explained that the primary targeting of NP to the nascent RNA easily occurs since there is no RNA target other than the nascent RNA in our system. However, it is worth noting that encapsidation of longer nascent cRNA by NP was not achieved when NP was simply added to the system (lane 4). This raises a question of how the newly synthesized virus genome is encapsidated with NP free of RNA.

NP recognizes the phosphodiester backbone of ssRNA in a specific sequence-independent manner. We used, as the enzyme source, the vRNP containing authentic NP, which is bound to the template RNA. Thus, it is reasonably hypothesized that newly synthesized cRNA chains remain associated with the template RNP, possibly by partial hybridization of the nascent cRNA with template vRNA and/or the interaction of nascent cRNA with template-bound authentic NP instead of exogenous NP. To address this, we immunopurified the template-bound authentic NP of vRNP in the presence of exogenous His-NP using anti-NP antibody (Fig. 2B). The length of RNA products associated with authentic NP or both authentic NP and exogenous His-NP (lane 3) was clearly distinct from that of RNA products interacting with only exogenous His-NP (lane 4). From these results, it is assumed that the nascent cRNA product is hardly encapsidated with exogenous NP since the nascent cRNA tends to interact more with template-bound NP than exogenous NP and might partially hybridize with the template.

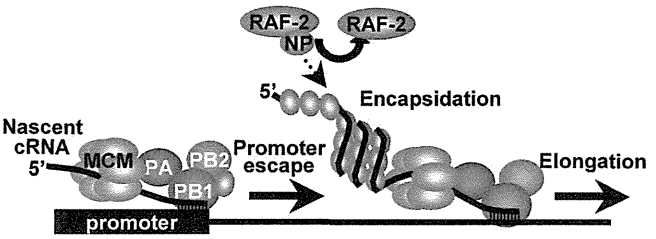

FIG. 4. Proposed model. NP facilitates the promoter escaping from the viral polymerase through the interaction between NP and the viral polymerase in an RNA binding activity-independent manner. During elongation step, RAF-2p48/UAP56 stimulates the coreplicational encapsidation of newly synthesized cRNA with exogenous NP, thereby increasing the processivity of the viral polymerase.

Encapsidation with NP mediated by RAF-2p48/UAP56. As shown in Fig. 2, it is assumed that some factor(s) may be missing in the encapsidation of nascent cRNA products with exogenous NP. Previously, RAF-2p48/UAP56/BAT1 (here, designated RAF-2p48/UAP56) belonging to the DExD-box family of ATP-dependent RNA helicase (13), also reported as NPI-5 (20), was identified as a host factor that binds to NP and stimulates influenza virus RNA synthesis from exogenously added model vRNA templates (16) and that is involved in splicing of cellular pre-mRNAs and messenger RNP maturation of cellular and viral transcripts (4, 25, 29). RAF-2p48/UAP56 binds to NP free of RNA but not to an NP-RNA complex and facilitates NP-RNA complex formation as a molecular chaperone for NP. Therefore, it was proposed that RAF-2p48/UAP56 is involved in the arrangement of NP on the template. However, its precise roles, including the requirement for the encapsidation process, have not yet been uncovered. Thus, we tried to examine whether RAF-2p48/UAP56 facilitates the encapsidation of newly synthesized RNA with exogenous NP (Fig. 3A). We found that long nascent cRNA was encapsidated with exogenous NP by the addition of RAF-2p48/UAP56 (Fig. 3A, compare lane 4, in which RAF-2p48/UAP56 is present, with lane 3, in which RAF-2p48/UAP56 is absent). The ATP-dependent RNA unwinding activity of RAF-2p48/UAP56 was not required for the encapsidation of nascent chains since the encapsidation occurred in the presence of ATPγS, which is a nonhydrolyzable analog of ATP (data not shown). Therefore, we propose a model whereby RAF-2p48/UAP56 facilitates the formation of RNP complexes by coreplicationally transferring exogenous NP to the nascent cRNA chain. It is unlikely that RAF-2p48/UAP56 remodels secondary structures of template and newly synthesized cRNA by its potential RNA helicase activity (Fig. 4). Furthermore, RAF-2p48/UAP56 stimulated the elongation activity of the viral polymerase, possibly by facilitating the encapsidation of nascent cRNA (Fig. 3, lane 2). It is speculated that the coreplicational encapsidation of nascent cRNA by NP may prevent the premature termination of RNA synthesis by avoiding a secondary structure of nascent RNA, which is hypothesized to be one of the causative factors in the termination process of other RNA polymerases (10, 27). Therefore, it is possible that the encapsidation of the nascent RNA with exogenous NP mediated by RAF-2p48/UAP56 increases the processivity of the

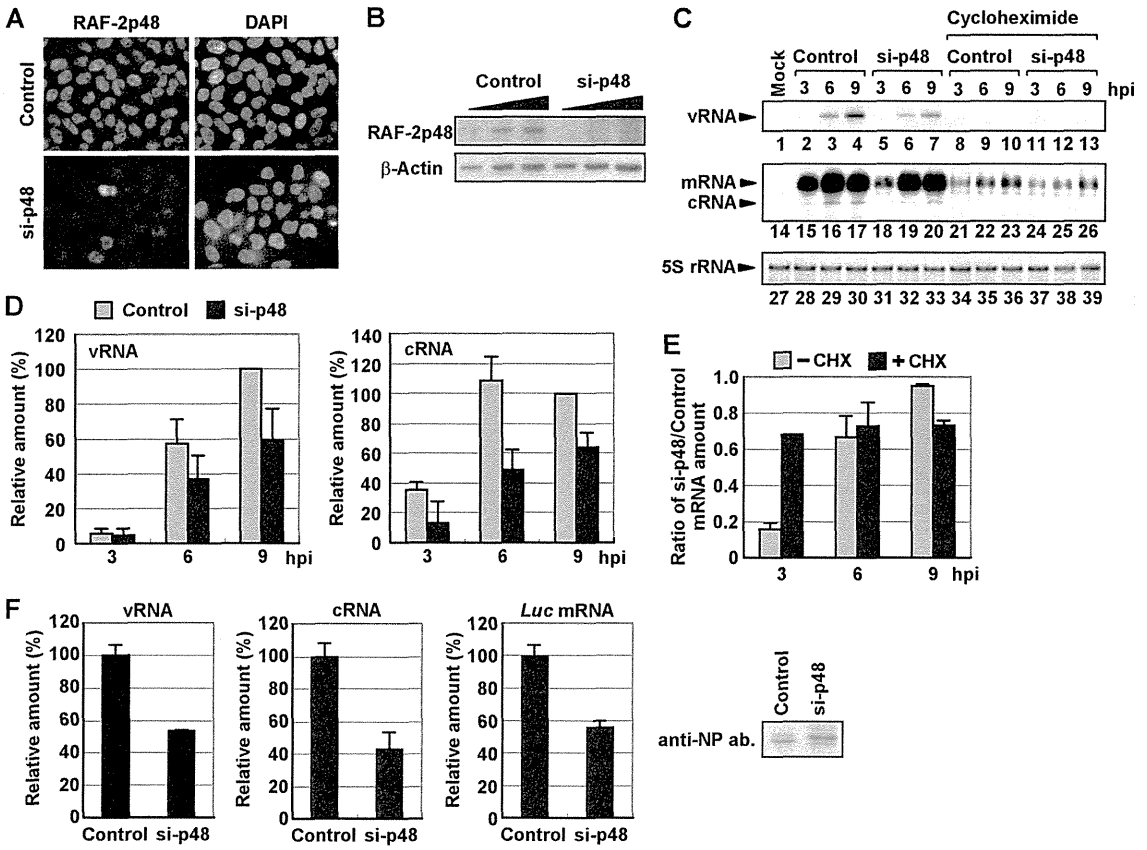

FIG. 5. Involvement of RAF-2p48/UAP56 in influenza virus genome replication in infected cells. (A) At 48 h posttransfection, cells transfected with either a control or siRNA against the RAF-2p48/UAP56 ORF (si-p48) were subjected to indirect immunofluorescence assay with anti-RAF-2p48/UAP56 antibody. Nuclear DNA stained with 4′,6-diamidino-2-phenylindole (DAPI) is also shown. Images were acquired under the same exposure time by a fluorescence microscope system (Axiovision; Carl Zeiss). (B) Expression level of RAF-2p48/UAP56. The lysates prepared from control and RAF-2p48/UAP56 knockdown cells (5×10^3, 1×10^4, and 2×10^4 cells) were separated by SDS-PAGE and then visualized by Western blotting assays with anti-NP and β-actin antibodies. (C, D, and E) Level of viral RNAs in infected RAF-2p48/UAP56 knockdown cells. Control and RAF-2p48/UAP56 knockdown cells were infected with influenza virus in the absence (lanes 1 to 7 and 14 to 20) or presence of cycloheximide (lanes 7 to 13 and 21 to 26) for 0, 3, 6, and 9 h. Primer extension assays were carried out with primers specific for segment 5 vRNA or m/cRNA as described in Materials and Methods. As a loading control, 5S rRNA was also detected (lanes 27 to 39). The band intensities were quantitatively measured by ImageJ software, and the results of three independent experiments are summarized in panel D and are indicated in panel E as the ratio of the mRNA amount in RAF-2p48/UAP56 knockdown cells to that in control cells with or without CHX. (F) The level of viral RNAs synthesized from a reconstituted model replicon in RAF-2p48/UAP56 knockdown cells. Control and RAF-2p48/UAP56 knockdown cells were transfected with plasmids expressing PB1, PB2, PA, and NP and model vRNA encoding the luciferase gene as described in Materials and Methods. At 12 h posttransfection, total RNAs were purified and then subjected to reverse transcription, followed by quantitative real-time PCR with primer sets specific for vRNA, cRNA, and luciferase mRNA. The expression level of NP protein in control and RAF-2p48/UAP56 knockdown cells was also detected by a Western blotting assay with anti-NP antibody (ab).

viral polymerase by avoiding inappropriate secondary structures of nascent cRNA.

Involvement of RAF-2p48/UAP56 in influenza virus genome replication in infected cells. Finally, we tried to examine whether RAF-2p48/UAP56 functions in influenza virus genome replication in cultured cells using siRNA-mediated gene silencing. At 48 h posttransfection of siRNA corresponding to the RAF-2p48/UAP56 ORF, the expression level of RAF-2p48/UAP56 in knockdown cells decreased to approximately 30% of that of cells transfected with the nontargeting siRNA used as a negative control (Fig. 5A and B). We carried out quantitative primer extension assays with appropriate primers specific for each vRNA and mRNA/cRNA of segment 5 (Fig. 5C and D). We confirmed that the product corresponding to cRNA was not found from a fraction bound with oligo(dT) cellulose (data not shown). This result showed that the accumulation of vRNA and cRNA was reduced and delayed in RAF-2p48/UAP56 knockdown cells compared with levels in control cells (Fig. 5C, lanes 1 to 7 and 14 to 20, and D). The same results were obtained for other segments (data not shown). It is proposed that nascent cRNA is degraded unless it is encapsidated with viral RNA polymerase and NP (33). In addition, the results shown in Fig. 3 and a previous report (16) demonstrated that RAF-2p48/UAP56 stimulates the viral polymerase activity. Thus, RAF-2p48/UAP56 might be involved in virus genome replication and encapsidation in infected cells. We also found that the level of NP mRNA in RAF-2p48/UAP56 knockdown cells decreased to 15% in control cells at 3 hpi (Fig. 5C, lanes 15 and 18, and E). In contrast, comparable amounts of NP mRNA were found in both control and RAF-

2p48/UAP56 knockdown cells at 6 and 9 hpi (Fig. 5C, lanes 16, 17, 19, and 20) since the amount of vRNA template sufficient for viral mRNA synthesis might be accumulated at 6 and 9 hpi, but the replication activity was reduced and delayed in RAF-2p48/UAP56 knockdown cells. To confirm the effect of RAF-2p48/UAP56 on viral transcription, we utilized cycloheximide (CHX), a potent protein synthesis inhibitor (Fig. 5C, lanes 8 to 13 and 21 to 26, and E). A previous report showed that CHX suppresses viral protein synthesis and thereby leads to degradation of replicated viral RNA but not mRNA since new vRNP formation was repressed (33). Therefore, we could examine the amount of viral mRNA synthesized from incoming vRNP independent of the level of vRNA accumulation in the presence of CHX (Fig. 5C, lanes 8 to 13, and E). The level of NP mRNA in RAF-2p48/UAP56 knockdown cells was reduced to 70% in control cells in the presence of CHX at 3 hpi (Fig. 5C, lanes 21 and 24, and E). Therefore, it is likely that the reduction of viral mRNA synthesis in RAF-2p48/UAP56 knockdown cells is mainly due to the decrease of vRNP accumulation in the absence of CHX although RAF-2p48/UAP56 has a stimulatory role in viral transcription, possibly by arrangement of NP on template and/or the nuclear export-competent messenger RNP formation (25). To rule out the possibility that the reduction of vRNA and cRNA synthesis was caused by the reduction of viral protein synthesis, we carried out a viral model replicon assay (19, 30) in which active vRNP complexes were reconstituted with PB1, PB2, PA, and NP and the model vRNA encoding the luciferase gene, as described in Materials and Methods (Fig. 5F). With this system, we could examine the viral polymerase activity independent of the expression level of viral proteins since viral proteins were expressed from plasmids under the control of cellular RNA polymerase II promoter in this assay. Results shown in Fig. 5F indicate that vRNA, cRNA, and viral mRNA synthesis was decreased in RAF-2p48/UAP56 knockdown cells compared with that in control cells even in the presence of comparable amounts of NP in both cells. We found that NP synthesized in RAF-2p48/UAP56 knockdown cells migrates differently from that in control cells (Fig. 5F). Previous reports showed that NP is modified by phosphorylation (23) and that its N-terminal region is digested by caspase (35), but the involvement of RAF-2p48/UAP56 in these is not known at present.

It is well known that NP is one of proteins responsible for virus genome replication (15, 18, 27, 33). Recently, it is reported that ubiquitination of NP regulates virus genome replication (12). It is proposed that the soluble viral polymerase might act as a replicative enzyme in *trans*, but transcription occurs from template-bound viral polymerase in *cis* (8). In this study and recent reports (9, 31–33), *de novo* cRNA synthesis is found from template-bound viral polymerase; thus, it could be explained that the soluble viral polymerase might have stimulatory activity but is not completely essential for the synthesis of nascent cRNA. The viral nuclear export protein (NEP/NS2) is also involved in the accumulation level of vRNA and cRNA (26). Further, it is reported that small noncoding RNAs derived from the influenza virus genome might regulate viral transcription and replication through their interaction with viral polymerase complexes (21). To further understand the mechanism of influenza viral genome replication, precise analyses of a functional replicative enzyme including viral and cellular factors are required.

ACKNOWLEDGMENTS

We thank Y. Ishimi (Ibaraki University) for the generous gifts of baculoviruses expressing MCM proteins. This research was supported in part by a grant-in-aid from the Ministry of Education, Culture, Sports, Science, and Technology of Japan (to K.N. and F.M.) and Research Fellowships of the Japanese Society for the Promotion of Science (to A.K.).

REFERENCES

1. **Biswas, S. K., P. L. Boutz, and D. P. Nayak.** 1998. Influenza virus nucleoprotein interacts with influenza virus polymerase proteins. J. Virol. **72:**5493–5501.
2. **Blumberg, B. M., M. Leppert, and D. Kolakofsky.** 1981. Interaction of VSV leader RNA and nucleocapsid protein may control VSV genome replication. Cell **23:**837–845.
3. **Chan, W. H., et al.** 2010. Functional analysis of the influenza virus H5N1 nucleoprotein tail loop reveals amino acids that are crucial for oligomerization and ribonucleoprotein activities. J. Virol. **84:**7337–7345.
4. **Fleckner, J., M. Zhang, J. Valcarcel, and M. R. Green.** 1997. U2AF65 recruits a novel human DEAD box protein required for the U2 snRNP-branchpoint interaction. Genes Dev. **11:**1864–1872.
5. **Honda, A., et al.** 1990. Purification and molecular structure of RNA polymerase from influenza virus A/PR8. J. Biochem. **107:**624–628.
6. **Honda, A., K. Ueda, K. Nagata, and A. Ishihama.** 1988. RNA polymerase of influenza virus: role of NP in RNA chain elongation. J. Biochem. **104:**1021–1026.
7. **Horikami, S. M., J. Curran, D. Kolakofsky, and S. A. Moyer.** 1992. Complexes of Sendai virus NP-P and P-L proteins are required for defective interfering particle genome replication in vitro. J. Virol. **66:**4901–4908.
8. **Jorba, N., R. Coloma, and J. Ortin.** 2009. Genetic trans-complementation establishes a new model for influenza virus RNA transcription and replication. PLoS Pathog. **5:**e1000462.
9. **Kawaguchi, A., and K. Nagata.** 2007. De novo replication of the influenza virus RNA genome is regulated by DNA replicative helicase, MCM. EMBO J. **26:**4566–4575.
10. **Komissarova, N., J. Becker, S. Solter, M. Kireeva, and M. Kashlev.** 2002. Shortening of RNA:DNA hybrid in the elongation complex of RNA polymerase is a prerequisite for transcription termination. Mol. Cell **10:**1151–1162.
11. **Labadie, K., E. Dos Santos Afonso, M. A. Rameix-Welti, S. van der Werf, and N. Naffakh.** 2007. Host-range determinants on the PB2 protein of influenza A viruses control the interaction between the viral polymerase and nucleoprotein in human cells. Virology **362:**271–282.
12. **Liao, T. L., C. Y. Wu, W. C. Su, K. S. Jeng, and M. M. Lai.** 2010. Ubiquitination and deubiquitination of NP protein regulates influenza A virus RNA replication. EMBO J. **29:**3879–3890.
13. **Linder, P., and F. Stutz.** 2001. mRNA export: travelling with DEAD box proteins. Curr. Biol. **11:**R961–R963.
14. **Masters, P. S., and A. K. Banerjee.** 1988. Complex formation with vesicular stomatitis virus phosphoprotein NS prevents binding of nucleocapsid protein N to nonspecific RNA. J. Virol. **62:**2658–2664.
15. **Medcalf, L., E. Poole, D. Elton, and P. Digard.** 1999. Temperature-sensitive lesions in two influenza A viruses defective for replicative transcription disrupt RNA binding by the nucleoprotein. J. Virol. **73:**7349–7356.
16. **Momose, F., et al.** 2001. Cellular splicing factor RAF-2p48/NPI-5/BAT1/UAP56 interacts with the influenza virus nucleoprotein and enhances viral RNA synthesis. J. Virol. **75:**1899–1908.
17. **Nagata, K., A. Kawaguchi, and T. Naito.** 2008. Host factors for replication and transcription of the influenza virus genome. Rev. Med. Virol. **18:**247–260.
18. **Newcomb, L. L., et al.** 2009. Interaction of the influenza a virus nucleocapsid protein with the viral RNA polymerase potentiates unprimed viral RNA replication. J. Virol. **83:**29–36.
19. **Obayashi, E., et al.** 2008. The structural basis for an essential subunit interaction in influenza virus RNA polymerase. Nature **454:**1127–1131.
20. **Palese, P., P. Wang, T. Wolff, and R. E. O'Neill.** 1997. Host-viral protein-protein interactions in influenza virus replication, p. 327–340. *In* M. A. McCrae (ed.), Molecular aspects of host-pathogen interaction. Cambridge University Press, Cambridge, United Kingdom.
21. **Perez, J. T., et al.** 2010. Influenza A virus-generated small RNAs regulate the switch from transcription to replication. Proc. Natl. Acad. Sci. U. S. A. **107:**11525–11530.
22. **Poole, E., D. Elton, L. Medcalf, and P. Digard.** 2004. Functional domains of the influenza A virus PB2 protein: identification of NP- and PB1-binding sites. Virology **321:**120–133.
23. **Portela, A., and P. Digard.** 2002. The influenza virus nucleoprotein: a multifunctional RNA-binding protein pivotal to virus replication. J. Gen. Virol. **83:**723–734.

24. **Qanungo, K. R., D. Shaji, M. Mathur, and A. K. Banerjee.** 2004. Two RNA polymerase complexes from vesicular stomatitis virus-infected cells that carry out transcription and replication of genome RNA. Proc. Natl. Acad. Sci. U. S. A. **101:**5952–5957.
25. **Read, E. K., and P. Digard.** 2010. Individual influenza A virus mRNAs show differential dependence on cellular NXF1/TAP for their nuclear export. J. Gen. Virol. **91:**1290–1301.
26. **Robb, N. C., M. Smith, F. T. Vreede, and E. Fodor.** 2009. NS2/NEP protein regulates transcription and replication of the influenza virus RNA genome. J. Gen. Virol. **90:**1398–1407.
27. **Shapiro, G. I., and R. M. Krug.** 1988. Influenza virus RNA replication in vitro: synthesis of viral template RNAs and virion RNAs in the absence of an added primer. J. Virol. **62:**2285–2290.
28. **Shimizu, K., H. Handa, S. Nakada, and K. Nagata.** 1994. Regulation of influenza virus RNA polymerase activity by cellular and viral factors. Nucleic Acids Res. **22:**5047–5053.
29. **Strasser, K., et al.** 2002. TREX is a conserved complex coupling transcription with messenger RNA export. Nature **417:**304–308.
30. **Sugiyama, K., et al.** 2009. Structural insight into the essential PB1-PB2 subunit contact of the influenza virus RNA polymerase. EMBO J. **28:**1803–1811.
31. **Vreede, F. T., and G. G. Brownlee.** 2007. Influenza virion-derived viral ribonucleoproteins synthesize both mRNA and cRNA in vitro. J. Virol. **81:**2196–2204.
32. **Vreede, F. T., H. Gifford, and G. G. Brownlee.** 2008. Role of initiating nucleoside triphosphate concentrations in the regulation of influenza virus replication and transcription. J. Virol. **82:**6902–6910.
33. **Vreede, F. T., T. E. Jung, and G. G. Brownlee.** 2004. Model suggesting that replication of influenza virus is regulated by stabilization of replicative intermediates. J. Virol. **78:**9568–9572.
34. **Yamanaka, K., A. Ishihama, and K. Nagata.** 1990. Reconstitution of influenza virus RNA-nucleoprotein complexes structurally resembling native viral ribonucleoprotein cores. J. Biol. Chem. **265:**11151–11155.
35. **Zhirnov, O. P., T. E. Konakova, W. Garten, and H. Klenk.** 1999. Caspase-dependent N-terminal cleavage of influenza virus nucleocapsid protein in infected cells. J. Virol. **73:**10158–10163.

JOURNAL OF VIROLOGY, Aug. 2011, p. 7504–7512 Vol. 85, No. 15
0022-538X/11/$12.00 doi:10.1128/JVI.02375-10

Recognition of Cap Structure by Influenza B Virus RNA Polymerase Is Less Dependent on the Methyl Residue than Recognition by Influenza A Virus Polymerase▽†

Chitose Wakai,[1,2] Minako Iwama,[2] Kiyohisa Mizumoto,[2,3] and Kyosuke Nagata[1]*

Department of Infection Biology, Graduate School of Comprehensive Human Sciences, University of Tsukuba, 1-1-1 Tennodai, Tsukuba 305-8575, Japan[1]; Department of Biochemistry, School of Pharmaceutical Sciences, Kitasato University, 5-9-1 Shirokane, Minato-ku, Tokyo 108-8641, Japan[2]; and Microbial Chemistry Research Center, 3-14-23 Kamiosaki, Shinagawa-ku, Tokyo 141-0021, Japan[3]

Received 12 November 2010/Accepted 10 May 2011

The cap-dependent endonuclease activity of the influenza virus RNA-dependent RNA polymerase cleaves host mRNAs to produce capped RNA fragments for primers to initiate viral mRNA synthesis. The influenza A virus (FluA) cap-dependent endonuclease preferentially recognizes the cap1 structure (m^7GpppNm). However, little is known about the substrate specificity of the influenza B virus (FluB) endonuclease. Here, we determined the substrate specificity of the FluB polymerase using purified viral RNPs and ^{32}P-labeled polyribonucleotides containing a variety of cap structures (m^7GpppGm, m^7GpppG, and GpppG). We found that the FluA polymerase cleaves m^7G-capped RNAs preferentially. In contrast, the FluB polymerase could efficiently cleave not only m^7G-capped RNAs but also unmethylated GpppG-RNAs. To identify a key amino acid(s) related to the cap recognition specificity of the PB2 subunit, the transcription activity of FluB polymerases containing mutated cap-binding domains was examined by use of a minireplicon assay system. In the case of FluA PB2, Phe323, His357, and Phe404, which stack the m^7GTP, and Glu361 and Lys376, which make hydrogen bonds with a guanine base, were essential for the transcription activity. In contrast, in the case of FluB PB2, the stacking interaction of Trp359 with a guanine base and putative hydrogen bonds using Gln325 and Glu363 were enough for the transcription activity. Taking these results together with the result for the cap-binding activity, we propose that the cap recognition pocket of FluB PB2 does not have the specificity for m^7G-cap structures and thus is more flexible to accept various cap structures than FluA PB2.

Influenza A virus (FluA) and influenza B virus (FluB) belong to the family of *Orthomyxoviridae*. The genomes of FluA and FluB are composed of a set of eight segments of RNA (vRNA) of negative polarity. vRNA is complexed with nucleoprotein (NP) and associated with the RNA polymerase to form viral ribonucleoprotein (vRNP) complexes. vRNP is an essential unit for both transcription and replication (9). In transcription, the RNA polymerase catalyzes not only RNA polymerization and polyadenylation of mRNA but also cleavage of host mRNAs to generate capped RNA fragments. The RNA polymerase is composed of one molecule each of three viral proteins, PB1, PB2, and PA. PB1 plays central roles in both RNA polymerase assembly (27, 31) and RNA polymerization (6). It contains the conserved motifs characteristic of RNA-dependent RNA polymerases and is directly involved in RNA chain elongation (1, 2). It binds to 5′- and 3′-terminal sequences of vRNA and cRNA (cRNA to vRNA), which are conserved in all segments and act as *cis*-acting elements for the viral RNA synthesis. PB2 is required for transcription and binds to the cap structures of host mRNAs. Recently, the structural features of the cap-binding site in FluA PB2 and the FluA PB1-PB2 contact site have been determined by functional studies and crystallography (12, 31). PA is involved in not only virus genome replication but also transcription as an endonuclease for generation of primers for RNA synthesis (8, 10, 13, 19, 36). It is also reported that PA is important for the polymerase assembly (19). The structure of the PB1-PA contact site has also been determined crystallographically (14, 27).

The FluA polymerase exhibits a cap-dependent endonuclease activity, which cleaves host mRNAs to produce capped RNA fragments with lengths of 11 to 13 nucleotides (nt). The resulting capped RNA fragment serves as a primer to initiate viral mRNA synthesis. It is well known that in the case of the FluA polymerase, eukaryotic mRNAs containing m^7G(5′)ppp(5′)Nm (cap1) and m^7G(5′)ppp(5′)NmN′m (cap2) structures stimulate *in vitro* viral RNA transcription strongly (4, 5, 29). Removal of m^7G of the cap from mRNA eliminates the priming activity, and naturally occurring uncapped mRNAs do not prime transcription (5, 29). In addition, the presence of methyl groups in the cap is required for the priming activity; reovirus mRNAs with 5′-terminal GpppG are inactive as primers (3). It has also been demonstrated that each of the two methyl groups in the cap1 structure, the 7-methyl residue of guanine and the 2′-*O*-methyl on the ribose of guanosine, strongly influences the capped RNA-primed transcription activity (4).

Biochemical and structural studies revealed the functional structures of the cap-binding proteins, including FluA PB2 (12), human translation initiation factor 4E (eIF4E) (33, 34),

* Corresponding author. Mailing address: Department of Infection Biology, Graduate School of Comprehensive Human Sciences, University of Tsukuba, 1-1-1 Tennodai, Tsukuba 305-8575, Japan. Phone and fax: 81-29-853-3233. E-mail: knagata@md.tsukuba.ac.jp.

† Supplemental material for this article may be found at http://jvi.asm.org/.

▽ Published ahead of print on 18 May 2011.

human nuclear cap-binding protein 20 (CBP20) (23), and vaccinia virus (nucleoside-2′-*O*-)-methyltransferase (VP39) (16). The overall structures of these four cap-binding proteins differ widely due to their evolutionarily unrelated origins, but the cap-binding pockets form a common structure and preferentially bind to the 7-methylated cap structure. These cap-binding proteins hardly bind to the unmethylated cap structure.

Most of our knowledge on the transcription mechanism of the influenza virus genome has been derived from studies on the FluA polymerase, whereas little is known about the FluB polymerase. It is reported that α-amanitin, a potent inhibitor for the host cell RNA polymerase II, inhibits influenza virus transcription, suggesting that eukaryotic mRNAs containing the cap structure are essential for influenza virus transcription (21). Using α-amanitin, we found that the growth of FluB is more sensitive to the amount of cellular mRNA than that of FluA (data not shown). To elucidate the transcription initiation mechanism of the FluB polymerase, we tried to determine the specificity of cap recognition by the FluB polymerase. First, we compared the substrate specificities of FluA and FluB polymerases using purified vRNPs and various capped RNA substrates (m^7GpppGm-, m^7GpppG-, and GpppG-RNA) and found that the FluB polymerase efficiently cleaves not only m^7G-capped RNAs but also unmethylated GpppG-RNA, whereas the FluA polymerase cleaves m^7G-capped RNAs specifically. We then tried to identify key amino acids related to the cap recognition of FluB PB2. In order to examine the transcription activity using mutated PB2 proteins, we utilized FluA and FluB minireplicon assay systems using a virus polymerase-dependent reporter gene (17, 35). The minireplicon system has been utilized for a number of functional analyses of *cis*-acting elements with the viral genome and *trans*-acting viral factors (10, 35). The reporter gene contains a coding region flanked by each viral 5′ and 3′ untranslated region (UTR), which function as promoters, and therefore mimics an influenza virus genomic segment. Using this assay system, we identified the important amino acids required for the cap recognition by the FluB polymerase by referencing functionally important amino acids in the FluA polymerase (12).

Based on the findings using the assay systems, we propose that the FluB polymerase possesses a novel cap recognition mechanism, which is different not only from the FluA polymerase but also from well-known cap-binding proteins. These findings could be important to develop novel anti-influenza virus drugs targeting the cap recognition and cleavage reaction.

MATERIALS AND METHODS

Biological materials. Monolayer cultures of 293T and MDCK cells were maintained at 37°C in Dulbecco's modified Eagle medium (DMEM) and minimal essential medium (MEM) (Nissui), respectively, supplemented with 10% fetal calf serum (Cell Culture Technologies). Influenza virus A/Panama/2007/99 (A/PA/99) and B/Shanghai/361/2002 (B/SH/02) were kindly supplied by Y. Suzuki and T. Gotanda (Kitasato Institute, Research Center for Biologicals, Saitama, Japan). Vaccinia virus capping enzyme and recombinant human mRNA (guanine-7-)methyltransferase (rhMTase) were prepared according to a previously described procedure (28).

Cloning of cDNAs for viral RNA polymerase subunits and nucleoprotein cDNA. For construction of mammalian expression vectors for influenza virus polymerase subunits (PB1, PB2, and PA) and nucleoprotein (NP), cDNAs corresponding to the full-length PB1, PB2 with a FLAG tag at its C terminus (PB2cFLAG), PA, and NP were amplified by reverse transcription-PCR (RT-PCR) from vRNAs of influenza virus A/PA/99 and B/SH/02 as templates using the following sets of phosphorylated primers (see Table S1 in the supplemental material): A-PB1-FOR and A-PB1-REV for FluA-PB1, A-PB2-FOR and A-PB2-cFLAG-REV for FluA-PB2cFLAG, A-PA-FOR and A-PA-REV for FluA-PA, A-NP-FOR and A-NP-REV for FluA-NP, B-PB1-FOR and B-PB1-REV for FluB-PB1, B-PB2-FOR and B-PB2-cFLAG-REV for FluB-PB2cFLAG, B-PA-FOR and B-PA-REV for FluB-PA, and B-NP-FOR and B-NP-REV for FluB-NP. The PCR products were then cloned into the EcoRV site of pCAGGS-P7 (7), resulting in construction of pCAGGS-Panama-PB1, pCAGGS-Panama-PB2-cFLAG, pCAGGS-Panama-PA, pCAGGS-Panama-NP, pCAGGS-Shanghai-PB1, pCAGGS-Shanghai-PB2-cFLAG, pCAGGS-Shanghai-PA, and pCAGGS-Shanghai-NP. cDNAs for PB2 mutants were prepared by site-directed mutagenesis using the primer sets for FluA-PB2-cFLAG and FluB-PB2-cFLAG and mutant primer sets (see Table S2 in the supplemental material). The PB2 mutant genes have been fully sequenced by standard methods (35).

Preparation of influenza virus vRNP. To prepare vRNP, we first treated purified influenza virus virions at 30°C for 60 min with a disruption buffer consisting of 50 mM Tris-HCl (pH 8.0), 100 mM KCl, 5 mM $MgCl_2$, 1 mM dithiothreitol (DTT), 5% glycerol, 2% Triton X-100, and 2% lysolecithin according to a method described previously (32). The sample was then directly subjected to centrifugation on a 30 to 60% (wt/vol) linear gradient of glycerol on a 70% (wt/vol) glycerol cushion in 50 mM Tris-HCl (pH 8.0) and 150 mM NaCl in a Beckman MLS-50 rotor with adapters at 163,000 × g_{AV} for 3 h at 4°C. Fractionation was carried out from the top of the gradient. Fractions containing vRNP were pooled and then used for *in vitro* endonuclease and elongation assays.

Preparation of various RNA substrates. Triphosphate-ended RNA with the 33-nucleotide sequence 5′-GAAAAAAAAAAAAAAAAAAAAAAAAAAAAUAAA-3′, designated pppG-RNA, was synthesized by using T7 RNA polymerase (Amersham Biosciences) and a synthetic DNA template. The protocol was previously described (30). Briefly, to prepare the template for the T7 RNA polymerase, the oligonucleotide T7P (5′-TAATACGACTCACTATA-3′), corresponding to the T7 promoter (−17 to −1), was annealed to the template oligonucleotide T7-polyA-R1 (5′-TTTATTTTTTTTTTTTTTTTTTTTTTTTTTCTATAGTGAGTCGTATTA-3′, where the underlined sequence is complementary to the T7 promoter [−17 to −1]). After the transcription reaction, the transcription mixture was treated with DNase I (Roche Applied Science). RNA was then extracted with phenol-chloroform, ethanol precipitated, and used as a capping substrate. To synthesize m^7G[^{32}P]pppGm-RNA and G[^{32}P]pppG-RNA, 50 pmol of pppG-RNA was incubated at 37°C for 2 h in the presence of 8 μM [α-^{32}P]GTP (800 cpm/fmol) and an appropriate amount of purified vaccinia virus capping enzyme, which has guanylyltransferase, guanine-7-methyltransferase, and ribose-2′-*O*-methyl-transferase activities, in a reaction mixture (50 μl) containing 50 mM Tris-HCl (pH 7.9), 2 mM $MgCl_2$, 40 mM NaCl, and 20 mM DTT in the presence or absence of 150 μM *S*-adenosyl-L-methionine (AdoMet). After the reaction, capped RNA was extracted with phenol-chloroform, ethanol precipitated, and dissolved in H_2O. To synthesize m^7G[^{32}P]pppG-RNA, 0.4 pmol of G[^{32}P]pppG-RNA was incubated at 30°C for 20 min with 15 ng/μl of rhMTase in a reaction mixture (20 μl) containing 25 mM Tris-HCl (pH 7.9), 0.5 mM DTT, 0.1 mg/ml bovine serum albumin (BSA), and 50 μM AdoMet. The RNA was extracted with phenol-chloroform, ethanol precipitated, and dissolved in H_2O. To confirm the cap structure on the synthesized RNA, the cap structure of the synthesized ^{32}P-capped RNA was liberated by digestion with nuclease P_1 (Wako) (28). The reaction product was analyzed by thin-layer chromatography (TLC) on a polyethyleneimine (PEI)-cellulose plate (PEI-CEL UV_{254}; Macherey-Nagel) with 0.65 M LiCl and visualized by autoradiography.

***In vitro* capped RNA cleavage and RNA elongation reactions.** The determination of Flu cap-dependent endonuclease activity and the subsequent RNA elongation reaction were carried out in a reaction mixture (25 μl) containing 50 mM Tris-HCl (pH 7.9), 0.1 mM ammonium acetate, 5 mM $MgCl_2$, 2.5 mM DTT, 0.1% Nonidet P-40, 8 U of RNasin, 3 to 5 fmol of each ^{32}P-capped RNA (800 cpm/fmol), and an appropriate amount of purified vRNPs without or with ATP, UTP, GTP, or CTP. The reaction mixture was incubated at 30°C for 2 h, and then RNA products were extracted with phenol-chloroform and ethanol precipitated. The RNA products denatured with formamide were electrophoresed in a 20% acrylamide gel containing 8 M urea. After electrophoresis, the gel was dried, and RNAs were visualized by autoradiography. The amount of synthesized RNA was measured with a liquid scintillation counter (LS6000IC; Beckman). The endonuclease activity was represented as a ratio of the amount of cleaved RNAs to that of total capped RNAs, and the RNA elongation efficiency was represented as a ratio of the amount of transcripts to that of total capped RNAs.

Cap-binding assay. UV cross-linking was carried out to measure the cap-binding activity of viral RNA polymerases. A reaction mixture (12 μl) containing

50 mM Tris-HCl (pH 7.9), 0.1 mM ammonium acetate, 5 mM $MgCl_2$, 2.5 mM DTT, 250 fmol of uncapped RNA substrate, 50 fmol of each ^{32}P-capped RNA (~800 cpm/fmol), and an appropriate amount of purified vRNPs was incubated for 30 min on ice and then irradiated on ice for 10 min with 254-nm UV light (FUNA-UV-Linker FS-1500 [Funakoshi, Japan]) with 0.2 mg/ml of heparin. The ^{32}P-labeled products were digested with nuclease P_1, analyzed by 6% SDS-PAGE, and detected by autoradiography.

Minireplicon assay. Two plasmid vectors carrying a reporter gene (an artificial influenza virus genome containing the firefly luciferase gene of negative polarity, which is synthesized in cells by the human DNA-dependent RNA polymerase I [Pol I]), were constructed as described previously (35). A fragment containing the luciferase gene sandwiched by 5′- and 3′-terminal sequences of FluA/PA/99 and FluB/SH/02 segment 8 was amplified by PCR with specific primers 5′-GTAGTAGAAACAAGGGTGTTTTTTACTCGAGATCTTACAATTTGGACTTTCCGCCCTT-3′ and 5′-GATCCGTCTCCGGGAGCAAAAGCAGGGTGACAAAGACATAATGCATATGGAAGACGCCAAAAACATAAAGAAAGG-3′ for FluA/PA/99 and 5′-TATTCGTCTCAGGGAGCAGAAGCAGAGGATTTGTTTAGTCACTGGCAAACGGAAAAAAATGGAAGACGCCAAAAACATAAAG-3′ and 5′-ATATCGTCTCGTATTAGTAGTAACAAGAGGATTTTTATTTTAAATTTACAATTTGGACTTTCCGCC-3′ for FluB/SH/02, using pGV-B (the promoterless luciferase reporter vector; Toyo Inc.) as a template. The amplified PCR products were digested with BsmBI and cloned into pHH21 containing the promoter region of the human rRNA gene (24, 25), which had been digested with BsmBI. The constructed plasmids were designated pHH-A-vNS-Luc and pHH-B-vNS-Luc, in which the luciferase gene in reverse orientation sandwiched with 23- and 26-nucleotide 5′- and 3′-terminal sequences of the FluA/PA/99 segment 8 or 30 and 44-nucleotide 5′- and 3′-terminal sequences of the FluB/SH/02 segment 8, respectively, is placed under the control of the human Pol I promoter. 293T cells were transfected with plasmids for the expression of the FluA minireplicon (pCAGGS-Panama-PB1, pCAGGS-Panama-PB2-cFLAG, pCAGGS-Panama-PA, pCAGGS-Panama-NP, and pHH-A-vNS-Luc) or FluB minireplicon (pCAGGS-Shanghai-PB1, pCAGGS-Shanghai-PB2-cFLAG, pCAGGS-Shanghai-PA, pCAGGS-Shanghai-NP, and pHH-B-vNS-Luc). A plasmid for the expression of *Renilla* luciferase driven by the simian virus 40 (SV40) promoter was used as an internal control for the dual-luciferase assay. As a negative control, 293T cells were transfected with the same plasmids, except for the omission of the PB2 expression plasmid. After transfection, the cells were incubated at 37°C for 24 h, and then the luciferase activity was determined using commercially available reagents (Promega) according to the manufacturer's protocol. The relative luminescence intensity was measured with a luminometer for 20 s. To measure the levels of accumulation of viral mRNA, cRNA, and vRNA, quantitative RT-PCR was performed. Total RNA was extracted from transfected cells and then reverse transcribed with either (i) oligo(dT)$_{20}$ for synthesizing cDNA from viral mRNA, (ii) 5′-ATATCGTCTCGTATTAGTAGTAACAAGAGCATT-3′, which is complementary to the 3′ portion of cRNA of the reporter gene, for synthesizing cDNA from cRNA, or (iii) 5′-TCCATCACGGTTTTGGAATGTTTACTACAC-3′, which is complementary to vRNA, for synthesizing cDNA from vRNA of the reporter gene. These single-stranded cDNAs were subjected to real-time quantitative PCR analyses (Thermal Cycler Dice real-time system TP800; TaKaRa) with SYBR Premix Ex *Taq* (TaKaRa) and two specific primers, 5′-TCCATCACGGTTTTGGAATGTTTACTACAC-3′, corresponding to the firefly luciferase mRNA between nucleotide sequence positions 728 and 757, and 5′-GTGCGCCCCCAGAAGCAATTTC-3′, which is complementary to the firefly luciferase mRNA between nucleotide sequence positions 931 and 952. *Renilla* luciferase mRNA was also amplified with two specific primers, 5′-GCAGCATATCTTGAACCATTC-3′, corresponding to the *Renilla* luciferase mRNA between nucleotide sequence positions 598 and 618, and 5′-CATCACTTGCACGTAGATAAG-3′, which is complementary to the *Renilla* luciferase mRNA between nucleotide sequence positions 725 and 745. The relative amounts of mRNA, cRNA, and vRNA were calculated by using the second-derivative maximum method and normalized to the amount of *Renilla* luciferase mRNA. The ratio of the amounts of mRNA and cRNA relative to vRNA is shown.

Detection of capped RNA coprecipitated with the viral RNA polymerase. 293T cells were transfected with plasmids for the expression of the FluB viral proteins, PB1, FLAG-tagged PB2 (wild-type or mutated PB2), and PA. At 24 h posttransfection, cells were resuspended in a lysis buffer (20 mM Tris-HCl [pH 7.9], 100 mM NaCl, 30 mM KCl, and 0.1% Nonidet P-40). The RNA polymerase complex composed of PB1, FLAG-tagged PB2, and PA was purified by incubation with anti-FLAG M2 agarose (Sigma) at 4°C for 3 h and eluted with an elution buffer (50 mM Tris-HCl [pH 7.9], 100 mM ammonium acetate, 5 mM $MgCl_2$, and 10% [vol/vol] glycerol) containing 0.1 mg/ml FLAG peptide (Sigma). RNAs which interact with the viral RNA polymerase was extracted from recombinant RNA polymerase complexes (100 ng of PB1 equivalents) with phenol-chloroform and ethanol precipitated with 20 μg of carrier tRNA. After treatment with calf intestinal alkaline phosphatase (CIAP), which removes free phosphate groups, periodate oxidation under mild conditions followed by β-elimination with aniline was carried out to remove 5′-terminal m^{7}G from capped RNA, generating RNA with 5′-triphosphate, which is the substrate for vaccinia virus capping enzyme, as described previously (4, 11). The RNA was then recapped using vaccinia virus capping enzyme with [α-^{32}P]GTP as described in the previous section. To measure the amount of ^{32}P-labeled capped RNA, the RNA was digested with tobacco acid pyrophosphatase (TAP) (Sigma) at 37°C for 1 h in a buffer containing 50 mM sodium acetate (pH 5.5), 5 mM EDTA, and 10 mM 2-mercaptoethanol. The reaction product was analyzed by thin-layer chromatography on a PEI-cellulose plate as described above, and the amount of [^{32}P]m^{7}Gp was measured with a liquid scintillation counter.

RESULTS

***In vitro* capped RNA cleavage reaction and subsequent RNA elongation reaction.** The FluA polymerase requires the cap1 structure (m^{7}GpppNm) stringently for transcription (4). In contrast, little is known about the requirement for the cap structure of the FluB polymerase. Thus, we first examined the efficiency of the capped RNA cleavage reaction and subsequent RNA elongation reaction by FluA and FluB polymerases using cap1-RNA (m^{7}GpppGm-RNA). The cap1-RNA labeled with ^{32}P in the cap structure was incubated with purified vRNP (see Fig. S1A in the supplemental material) in the absence or presence of nucleoside triphosphates (NTPs) (Fig. 1A). RNA products were analyzed by 15% PAGE containing 8 M urea. FluA and FluB polymerases cleaved the cap1-RNA and produced 11- to 13-nucleotide and 11- to 12-nucleotide RNAs, respectively, in the absence of NTPs (Fig. 1A, lanes 2 to 7), indicating that the endonuclease activity of FluB is different from that of FluA in the distance of cleavage site from the cap structure. This cleavage pattern was observed commonly among FluA strains and among FluB strains (see Fig. S1B, lanes 2 to 6, in the supplemental material). The cleaved RNA products were elongated in the presence of NTPs in a dose-dependent manner (Fig. 1A, lanes 8 to 13), but the elongation efficiency of the FluB polymerase was lower than that of the FluA polymerase. We also confirmed that these elongated products contain full-length transcripts from 8 segments and are partially polyadenylated (see Fig. S2 in the supplemental material). To investigate the cap-binding activity of the polymerases, UV cross-linking assays were carried out (Fig. 1B). Cap1-RNA specifically bound to PB2 in both the FluA and FluB polymerases, although the cap-binding activity of FluB PB2 is less (~25%) than that of FluA PB2. These results suggest that the FluA and FluB polymerases are different in their binding to RNA containing the cap1 structure and in their cleavage modes.

Specificity of recognition of cap structures by Flu polymerases. To investigate the specificity of recognition of cap structures by FluA and FluB polymerases, we carried out similar experiments using RNA primers containing various cap structures. To this end, we prepared ^{32}P-labeled RNAs containing differently methylated cap structures, such as m^{7}GpppGm, m^{7}GpppG, and GpppG, as described in Materials and Methods. After preparation, we analyzed the terminal cap structure using nuclease-digested samples (see Materials and Methods) and thin-layer chromatography on a PEI-cellulose plate. As shown in Fig. 2A, we confirmed that each RNA

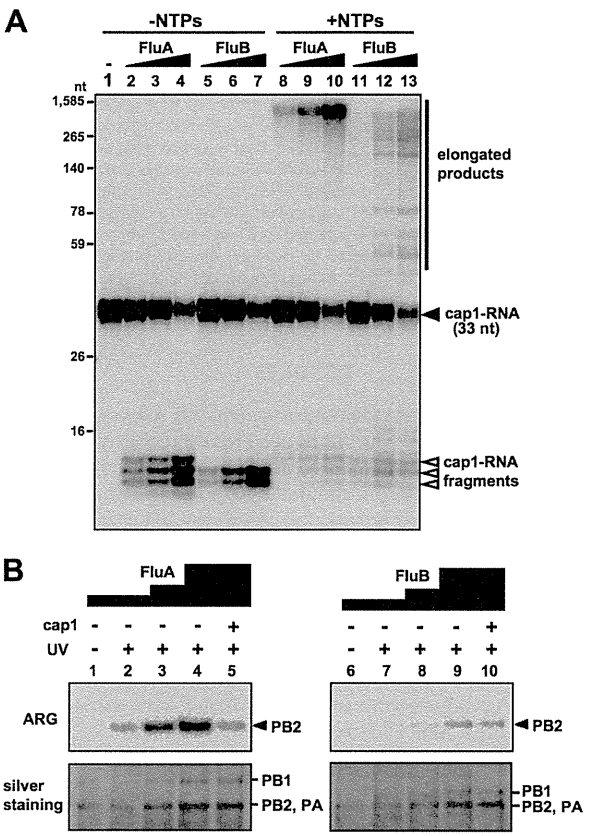

FIG. 1. *In vitro* capped RNA cleavage, RNA elongation and cap-binding reactions. (A) Dose dependency of *in vitro* capped RNA cleavage and subsequent RNA elongation by vRNP. *In vitro* capped RNA cleavage and RNA elongation reactions were performed with 20, 40, and 80 ng of FluA (lanes 2 to 4 and 8 to 10) and FluB (lanes 5 to 7 and 11 to 13) vRNP using 2 fmol of m^7GpppGm-RNA. Capped RNA cleavage was performed in the absence of NTPs (lanes 2 to 7), while RNA elongation was performed in the presence of NTPs (lanes 8 to 13). Synthesized RNA products were analyzed by 15% PAGE containing 8 M urea. (B) Interaction of vRNP with the cap1 structure. UV cross-linking was performed using 50, 100, and 200 ng of FluA (lanes 1 to 5) and FluB (lanes 6 to 10) vRNPs with (lanes 2 to 5 and 7 to 10) or without (lanes 1 and 6) UV irradiation at 254 nm. Competition experiments were performed in the presence of 100 pmol of m^7GpppGm analogue (lanes 5 and 10). Upper panels show autoradiography (ARG), while lower panels show silver staining patterns.

had the expected cap structure. Using these RNAs as substrates, we carried out *in vitro* capped RNA cleavage and subsequent RNA elongation reactions with FluA or FluB vRNPs. As expected, FluA vRNP specifically cleaved both m^7GpppGm-RNA and m^7GpppG-RNA, although the latter was less efficiently cleaved (Fig. 2B, lanes 2, 5, and 8, and D). The m^7GpppGm-RNA fragments were most successfully elongated into viral mRNAs (Fig. 2C, lane 2, and E). In contrast, FluB vRNP could cleave GpppG-RNA efficiently in addition to the m^7GpppGm-RNA and m^7GpppG-RNA (Fig. 2B, lanes 3, 6, and 9, and D). It is noteworthy that m^7GpppGm-RNA fragments also served as an efficient primer for chain elongation, as is the case for the FluA polymerase (Fig. 2C, lane 3, and E). Moreover, we carried out UV cross-linking assays using RNA primers containing various cap structures (Fig. 2F). Interestingly, the cap-binding activity was detected just using m^7GpppGm-RNA with both FluA and FluB vRNPs. These results indicate that the guanine-7-methyl residue is a key for stable cap binding of both FluA and FluB polymerases. It is also indicated that the cap-binding activity is strictly related to the elongation efficiency but not to the cleavage reaction. It is presently unknown why the binding of GpppG and m^7GpppG was not detected under the conditions employed, while m^7GpppG-RNA was recognized and cleaved by both FluA and FluB polymerases and GpppG-RNA was by the FluB polymerase. Since m^7GpppG-RNA and GpppG-RNA were not effective for elongation, the cleavage of these cap structures would be abortive for transcription, possibly due to improper recognition.

Identification of key amino acids involved in the cap recognition specificity of the PB2 subunit of the FluB polymerase. To clarify the cap recognition mechanism, we focused our structure-related functional studies on the interaction between the cap1 structure and the PB2 subunit, which has the cap-binding domain. It is quite likely that amino acid residues essential for cap binding are conserved between FluA and FluB (Fig. 3A). Three-dimensional (3D) structural studies (12) revealed that in the FluA PB2 cap-binding domain (Fig. 3B), Phe404 and His357 sandwich the methylated guanine and Phe323 stacks on the ribose of m^7GTP. Glu361 makes hydrogen bonds with the N1 and N2 positions of guanine, and Lys376 also makes a hydrogen bond with position O6 of guanine. Computer-associated modeling could make the FluB PB2 cap-binding domain fit on the FluA PB2 cap-binding domain (Fig. 3C). In the model of the FluB cap-binding domain, 2 amino acids, Gln325 and Trp359, are different from Phe323 and His357 of the FluA cap-binding domain, respectively.

To determine key amino acids related to the cap recognition specificity, the transcription activity was measured using a minireplicon assay system. In this assay system, we have used a transient-transfection system with a viral genome, in which the coding region for a viral gene is replaced with a luciferase reporter gene while *cis*-acting regulatory regions (24) remain intact (35). The cellular RNA polymerase I produces a negative-sense luciferase RNA sandwiched with viral terminal sequences. Luciferase mRNA is synthesized by transcription of the negative-sense RNA with the viral RNA polymerase and NP and subjected to translation. This system has been used to measure the transcription activity of the Flu polymerase (20, 22).

In the case of FluA PB2, His357, with which methylated guanine is stacked, could be replaced by other aromatic residues such as Trp and Phe, while Phe404, which is also involved in stacking methylated guanine, could not be (Fig. 4A). Leu could not substitute for either His357 and Phe404. On the other hand, in the case of FluB PB2, Trp359 could be replaced with other aromatic residues (but with less efficiency than for the FluA polymerase), but Phe406 could be replaced with hydrophobic residues such as Tyr and Leu (Fig. 4B). To confirm the importance of the hydrogen bonds with methylated guanine, Glu361 and Lys376 in FluA PB2 and Glu363 and Lys378 in FluB PB2 were replaced with alanine (Ala). Ala substitutions in FluA PB2 abolished the transcription activity,

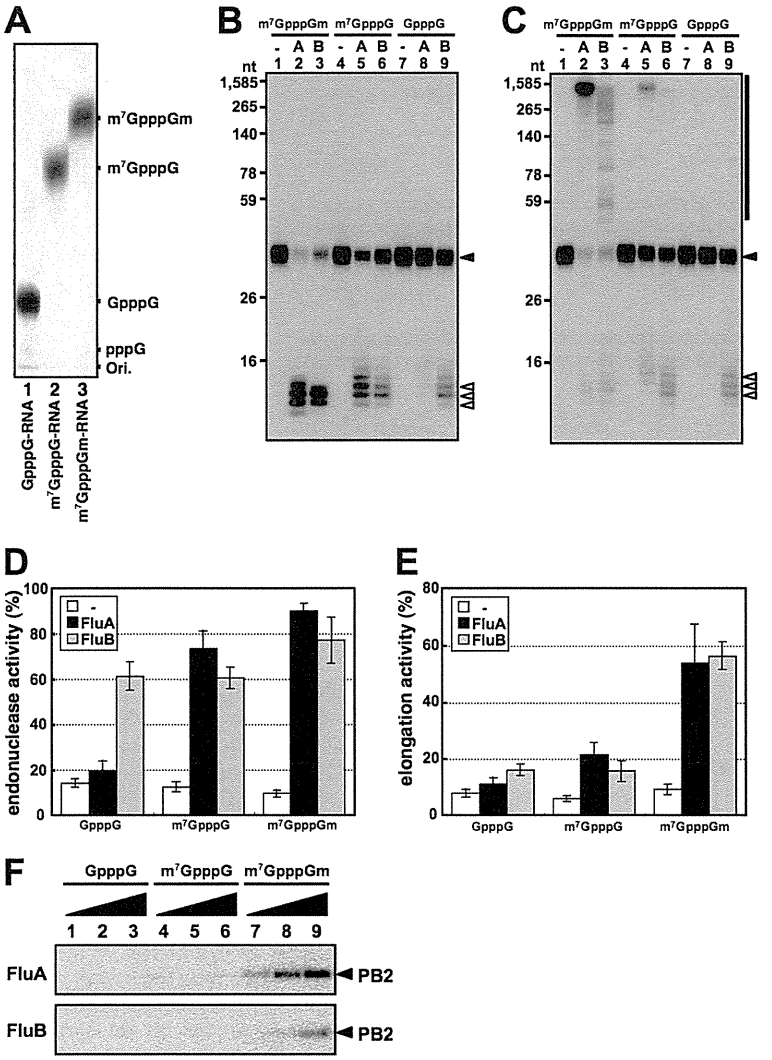

FIG. 2. Specificity of recognition of cap structures by Flu polymerases. (A) Analysis of 5′-terminal cap structures of RNAs. T7 RNA polymerase-synthesized RNAs were treated with nuclease P_1 and analyzed by TLC (PEI-CEL, 0.65 M LiCl), and radioactive nucleotides were detected by autoradiography. (B and C) *In vitro* capped RNA cleavage (B) and RNA elongation (C) reactions were performed with 600 ng of FluA (lanes 2, 5, and 8) or FluB (lanes 3, 6, and 9) vRNP using 2 fmol of variously methylated capped RNAs (m^7GpppGm-RNA, lanes 1 to 3; m^7GpppG-RNA, lanes 4 to 6; GpppG-RNA, lanes 7 to 9). RNA products were analyzed by 15% PAGE containing 8 M urea. The input capped RNAs (33 nt), the cleaved capped RNA products, and the elongated products are indicated as a closed triangle, open triangles, and a black bar, respectively, at the right. (D and E) Ratios of cleaved RNA products (D) and RNA transcripts (E) to total input primer RNAs. (F) Cap-binding activity for variously methylated capped RNAs. UV cross-linking was performed using 50, 100, and 200 ng of FluA (upper panel) and FluB (lower panel) vRNP and 50 fmol of variously methylated capped RNAs (GpppG-RNA, lanes 1 to 3; m^7GpppG-RNA, lanes 4 to 6; m^7GpppGm-RNA, lanes 7 to 9).

while Ala substitution for Lys378 of FluB PB2 caused only a small decrease in the transcription activity (Fig. 4C and D). These results suggest that the stacking interaction of His357 and Phe404 and the hydrogen bonds of Glu361 and Lys376 with methylated guanine are essential for cap recognition by the FluA polymerase. This is in good agreement with a previous report (12). In contrast, it is suggested that the stacking interaction of Trp359 and the hydrogen bonds of Glu363 with methylated guanine are sufficient for cap recognition by the FluB polymerase. These results indicate that the mechanism for recognition of methylated guanine by the FluB polymerase could be different from that for the FluA polymerase. It is also speculated that the cap-binding pocket of the FluB polymerase may be more flexible or less stringent than that of the FluA polymerase in recognition of various cap structures, since Phe406 of FluB PB2 is changeable with other amino acids.

Phe323 in FluA PB2 stacks on the ribose of m^7GTP and was essential for cap recognition (see Fig. S3 in the supplemental

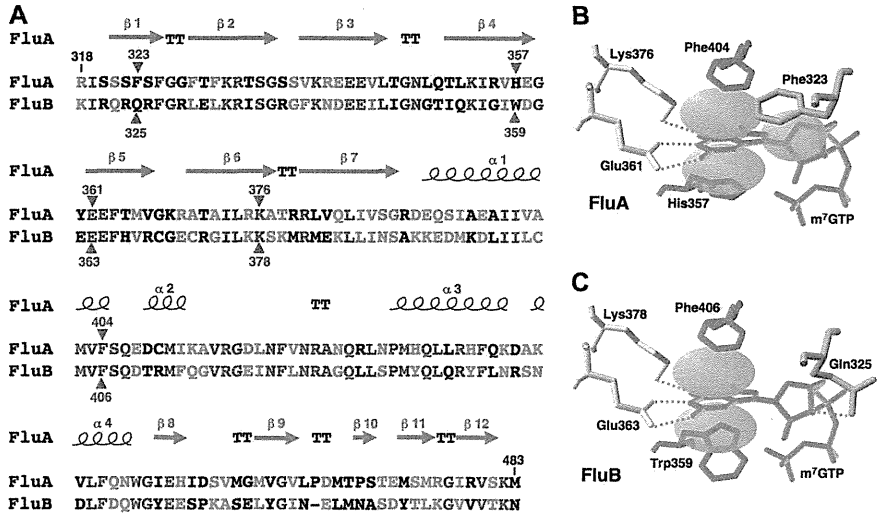

FIG. 3. Structure of the PB2 cap-binding domain. (A) Sequence alignment of the PB2 cap-binding domains of FluA (A/Panama/2007/99) and FluB (B/Shanghai/361/2002). The secondary structure of FluA is displayed over the sequence alignment. Blue letters and green letters show identical residues and similar residues, respectively. Purple triangles indicate the residues in contact with the cap analogue m^7GTP. (B and C) Model of m^7GTP interaction with the cap-binding domains of FluA PB2 (B) (10) and FluB PB2 (C) drawn by computer-associated calculation, with putative hydrogen bonds shown as green dotted lines.

material) (12). However, it is likely that Gln325 in FluB PB2, which is located in the same position of Phe323 in FluA PB2, makes a hydrogen bond with the ribose of m^7GTP. We speculated that FluB PB2 recognizes the cap structure in a flexible pocket as discussed above, so that the hydrogen bonds made by Gln325 and Glu363 could be more crucial for cap binding than those in FluA PB2. In addition, there could be an appropriate amino acid in the amino acid combination between amino acid positions 325 and 363 in FluB PB2 in order to keep the flexible pocket. To confirm this prediction, the transcription activities of mutants with substitutions at position 325 were examined in the presence of the Asp363 mutant (Fig. 4E). The transcription activity of the Asp363 single mutant was reduced to 20% of the wild-type level, possibly because of a longer distance between Asp363 and guanine residues for hydrogen bonds (Fig. 4E; see Fig. S4B in the supplemental material). Interestingly, Lys and Arg mutations but not Ala and Asn mutations at position 325 could rescue the transcription activity of Asp363 (Fig. 4E). We also examined the effect of an Asp363 single mutation and an Arg325-Asp363 double mutation on the transcription and replication processes and the cap-binding activity (Fig. 5). According to the levels of accumulation of mRNA (Fig. 5A) and cRNA (Fig. 5B), the level of reporter expression (Fig. 4E) is well correlated with the transcription but not the replication activities. To examine the cap-binding activity *in vivo*, capped RNAs that could interact with the viral RNA polymerase were coprecipitated from cells expressing the recombinant RNA polymerase, and the cap structure was detected by recapping of RNA which had been CIAP treated and then decapped (β-eliminated) (Fig. 5C). We could detect the [^{32}P]m^7Gp labeled by [α-^{32}P]GTP and vaccinia virus capping enzyme, depending on TAP digestion. In contrast, uncapped RNA treated with CIAP was poorly labeled by this protocol. These results indicate that this recapping method is suitable for the detection of capped RNA specifically. Using this method, we found that the cap-binding activities of these mutants (Fig. 5D) are well correlated with these transcription activities (Fig. 4E) and the mRNA accumulation levels (Fig. 5A). These results indicate that the Arg at position 325 in FluB PB2 supports cap recognition when Glu363 is replaced with Asp363.

DISCUSSION

Most of our knowledge on the transcription mechanism of the influenza virus genome has been derived from studies on FluA, while little has been demonstrated for FluB. This is also the case for studies on the enzymatic aspects of these viral RNA polymerases. Each of the two methyl groups in the cap1 structure, the 7-methyl residue of the guanine base and the 2′-*O*-methyl residue on the ribose of the penultimate base, strongly influences the transcription activity of the FluA polymerase (4). Recently, the structure of the PB2 cap-binding domain of the FluA polymerase with m^7GTP has been clarified (12). Based on these reports, we tried to identify the specificity of cap recognition and characterize key amino acids for cap recognition of the FluB polymerase.

First, we compared the efficiencies of capped RNA cleavage and subsequent RNA elongation reactions of the FluA polymerase with those of the FluB polymerase using cap1-RNA. As expected, the FluA polymerase exhibited efficient endonuclease activity, elongation activity, and cap-binding affinity. The pattern of cleavage of cap1-RNA by the FluB polymerase was different from that by the FluA polymerase (Fig. 1A; see Fig. S1B in the supplemental material), and the RNA elongation and cap-binding activities of the FluB polymerase were lower than those of the FluA polymerase (Fig. 1A and B). These results indicate that the cap binding and cleavage mechanism

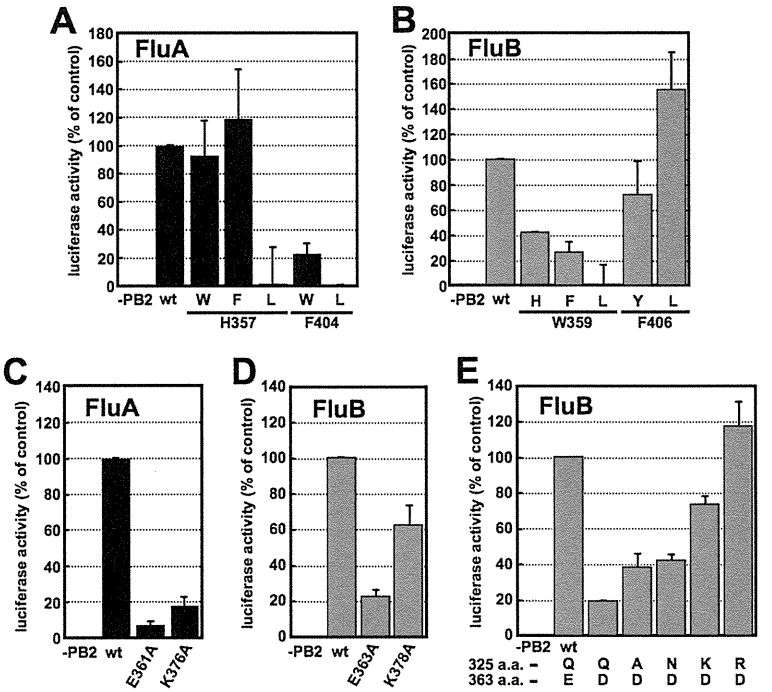

FIG. 4. Transcription activities of PB2 mutants in a minireplicon system. (A and B) Effects of mutations of m^7GTP stacking residues in FluA (A) and FluB (B) PB2 on transcription activity. (C and D) Effects of mutations in residues involved in hydrogen bonds with the guanine residue of m^7GTP in FluA (C) and FluB (D) PB2 on transcription activity. (E) Effect of mutations in Gln325 with an Asp mutation at position 363 in FluB PB2 on transcription activity. The firefly luciferase activity was normalized to *Renilla* luciferase activity. The results are averages and standard deviations (SD) from four independent experiments.

of the FluB polymerase are different from those of the FluA polymerase.

We then examined the specificity of recognition of cap structures by the FluB polymerase compared with that by the FluA polymerase. Using various methylated capped RNAs, we performed capped RNA cleavage and RNA elongation assays (Fig. 2). The FluA polymerase cleaved RNA containing m^7G specifically, while the FluB polymerase could cleave GpppG-RNA as well as RNA containing m^7G. Both the FluA and FluB polymerases elongated and bound to the cap structure efficiently only in the case of $m^7GpppGm$-RNA compared with other capped RNAs (Fig. 2C, 2E, and 2F). Based on these results, we propose that the FluA polymerase recognizes strictly the guanine-7-methyl residue in the cleavage reaction and that the FluB polymerase recognizes only the cap core structure (GpppX), which may result in its weak cap1-binding activity. In addition, these results suggest that the ribose 2′-*O*-methyl residue and/or the guanine-7-methyl residue may be responsible for the elongation reaction by both FluA and FluB polymerases, because cap binding and efficient elongation could not be observed except for $m^7GpppGm$-RNA.

To elucidate the mechanism of cap recognition by the FluB polymerase, we studied the PB2 subunit, which has the cap-binding domain. Recently, the 3D structure of the FluA PB2 cap-binding domain was revealed (12). Amino acid residues essential for cap binding were identified and found to be conserved between FluA and FluB polymerases (Fig. 3A). In the FluA PB2 cap-binding domain (Fig. 3B), the methylated guanine base is sandwiched with His357 and Phe404, and Phe323 stacks on the ribose of m^7GTP. Glu361 makes hydrogen bonds with the N1 and N2 positions of guanine, and Lys376 also makes hydrogen bonds with the O6 position of guanine. Based on the structure of the FluA PB2 cap-binding domain, a model of the FluB PB2 cap-binding domain was postulated (Fig. 3C). Five amino acids which contact the guanine-7-methyl residue are highlighted. Minireplicon assays showed that Trp359 in FluB PB2 is crucial for possible stacking interaction with a methylated guanine base without sandwiching with Phe406 (Fig. 4B). Moreover, the hydrogen bond made by Lys378 to the O6 position of guanine seemed not to be essential for cap recognition (Fig. 4D). These results suggest that the FluB polymerase recognizes the cap structure in a manner different from the FluA polymerase. We illustrated a new proposed computer-associated model for cap recognition by FluB PB2 (see Fig. S4A in the supplemental material), although the 3D structure of the FluB PB2 cap-binding domain has not been determined. The overall structures of four cap-binding proteins, FluA PB2 (12), eIF4E (33, 34), CBP20 (23), and VP39 (16), differ each other widely due to their evolutionarily unrelated origins, but the cap-binding pockets are essentially quite similar (see Fig. S5 in the supplemental material), although there are some differences in details. In addition to the two aromatic amino acids, an acidic residue is directed toward the pocket to accommodate the positively charged π-ring system of

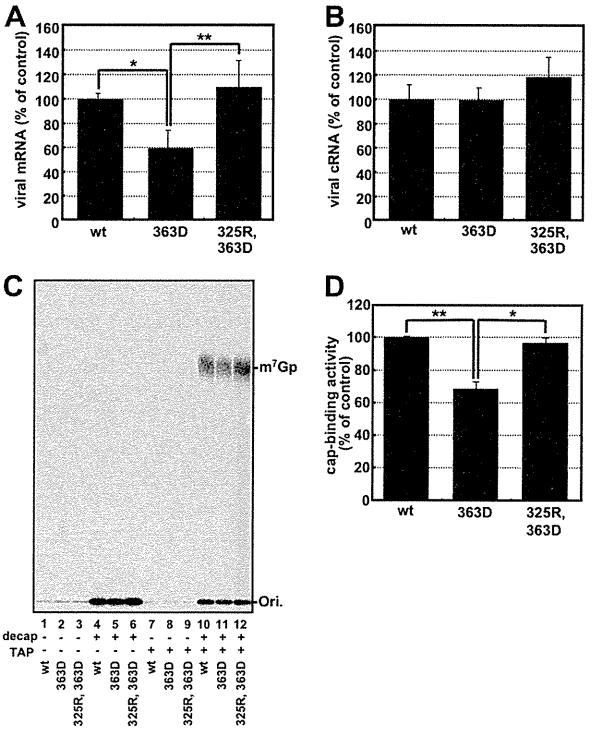

FIG. 5. Suppression mutation in transcription and cap-binding activities for the FluB PB2-363D mutant. (A and B) The levels of accumulation of viral mRNA (A) and cRNA (B) were measured by qPCR. (C) Cap-binding activities of mutants. Coprecipitated capped RNAs with 100 ng of recombinant RNA polymerase complexes (wild type [wt], lanes 1, 4, 7, and 10; 363D mutant, lanes 2, 5, 8, and 11; 325R-363D double mutant, lanes 3, 6, 9, and 12) were recapped before (lanes 1 to 3 and 7 to 9) and after (lanes 4 to 6 and 10 to 12) decapping by β-elimination. Recapped RNAs were treated without (lanes 1 to 6) or with (lanes 7 to 12) tobacco acid pyrophosphatase (TAP) and analyzed by TLC (PEI-CEL, 0.65 M LiCl), and radioactive nucleotides were determined by autoradiography. (D) The radioactivity of [^{32}P]m^{7}Gp of TAP-treated products which were recapped after decapping was counted with a liquid scintillation counter. The cap-binding activity is represented as a ratio to the amount of [^{32}P]m^{7}Gp derived from the wild type. These results are averages and SD from three independent experiments, and the level of significance was determined by Student's *t* test (unpaired) (*, $P < 0.0025$; **, $P < 0.0005$).

the methylated guanine. These amino acids provide high specificity for the recognition of m^{7}GTP and exhibit low affinity for nonmethylated cap analogues (>100-fold difference in affinity compared with N^7-methylated ones) (15, 18, 26). Compared with these well-known cap-binding proteins, the cap-binding pocket of FluB PB2 contains only one aromatic amino acid, Trp359. This feature may cause the low affinity of FluB PB2 for the cap1 structure (Fig. 1B) and the recognition of nonmethylated capped RNA (GpppG-RNA) (Fig. 2) compared with FluA PB2.

In the case of FluA PB2, the stacking interaction of Phe323 with the ribose of m^{7}GTP is also essential for cap recognition. However, Gln325 of FluB PB2 seems to make a hydrogen bond with the ribose of m^{7}GTP instead of a stacking interaction. To examine our speculation that FluB PB2 recognizes the cap structure in the flexible pocket, we made substitution mutations at position 325 in the presence of an Asp363 mutation (Gln → Asp), which should extend too much into the pocket where Gln325 is present. Interestingly, the transcription activity and the cap-binding activity of the Asp363 mutant were restored to the wild-type levels by the Arg325 mutation (Fig. 4E and 5) without changing the replication activity. The transcription activity of the Asp363 single mutant was decreased, possibly because the longer distance between Asp363 and the guanine residue may make hydrogen bonds weak (see Fig. S4B in the supplemental material). These results suggest that the hydrogen bond made by Arg325 with the ribose of the guanosine could support the recognition of the cap structure (Fig. 4E, 5A, 5C, and 5D; see Fig. S4C in the supplemental material). Crystal structure analyses of wild-type FluB PB2 and the mutant containing Arg325 and Asp363 are needed to support our hypothesis.

In summary, our results indicate that the substrate specificity and the residues essential in the cap recognition are different between FluA and FluB polymerases. In the case of the FluA polymerase, m^{7}G-capped RNA is cleaved specifically, and the stacking interactions of His357 and Phe404 with the methylated guanine base and of Phe323 with the ribose of m^{7}GTP and the hydrogen bonds made by Glu361 and Lys376 on the methylated guanine are essential for cap recognition as observed in other cap-binding proteins. In contrast, in the case of the FluB polymerase, unmethylated capped RNA is cleaved as well as m^{7}G-capped RNA, and the stacking interaction which is made only by Trp359 with the guanine base and the hydrogen bonds which are made by Glu363 on the guanine base and by Gln325 with the ribose of m^{7}GTP are enough for cap recognition.

ACKNOWLEDGMENTS

We thank Y. Suzuki and T. Gotanda (Kitasato Institute, Research Center for Biologicals, Saitama, Japan) for providing the purified influenza virus A/Panama/2007/99 and B/Shanghai/361/02 virions. We also thank T. Ogino (Lemer Research Institute, Cleveland Clinic, Cleveland, OH) and A. Kawaguchi (Kitasato Institute for Life Sciences, Kitasato University, Tokyo, Japan) for critical discussion.

This research was supported in part by a grant-in-aid from the Ministry of Education, Culture, Sports, Science, and Technology of Japan (to K.N.).

REFERENCES

1. **Argos, P.** 1988. A sequence motif in many polymerases. Nucleic Acids Res. **16:**9909–9916.
2. **Biswas, S. K., P. L. Boutz, and D. P. Nayak.** 1998. Influenza virus nucleoprotein interacts with influenza virus polymerase proteins. J. Virol. **72:**5493–5501.
3. **Bouloy, M., M. A. Morgan, A. J. Shatkin, and R. M. Krug.** 1979. Cap and internal nucleotides of reovirus mRNA primers are incorporated into influenza viral complementary RNA during transcription in vitro. J. Virol. **32:** 895–904.
4. **Bouloy, M., S. J. Plotch, and R. M. Krug.** 1980. Both the 7-methyl and the 2′-O-methyl groups in the cap of mRNA strongly influence its ability to act as primer for influenza virus RNA transcription. Proc. Natl. Acad. Sci. U. S. A. **77:**3952–3956.
5. **Bouloy, M., S. J. Plotch, and R. M. Krug.** 1978. Globin mRNAs are primers for the transcription of influenza viral RNA in vitro. Proc. Natl. Acad. Sci. U. S. A. **75:**4886–4890.
6. **Braam, J., I. Ulmanen, and R. M. Krug.** 1983. Molecular model of a eucaryotic transcription complex: functions and movements of influenza P proteins during capped RNA-primed transcription. Cell **34:**609–618.
7. **Chen, Z., et al.** 1998. Comparison of the ability of viral protein-expressing plasmid DNAs to protect against influenza. Vaccine **16:**1544–1549.
8. **Dias, A., et al.** 2009. The cap-snatching endonuclease of influenza virus polymerase resides in the PA subunit. Nature **458:**914–918.

9. **Engelhardt, O. G., and E. Fodor.** 2006. Functional association between viral and cellular transcription during influenza virus infection. Rev. Med. Virol. **16:**329–345.
10. **Fodor, E., et al.** 2002. A single amino acid mutation in the PA subunit of the influenza virus RNA polymerase inhibits endonucleolytic cleavage of capped RNAs. J. Virol. **76:**8989–9001.
11. **Fraenkel-Conrat, H., and A. Steinschneider.** 1967. Stepwise degradation of RNA: periodate followed by aniline cleavage. Methods Enzymol. **12B:**243–246.
12. **Guilligay, D., et al.** 2008. The structural basis for cap binding by influenza virus polymerase subunit PB2. Nat. Struct. Mol. Biol. **15:**500–506.
13. **Hara, K., F. I. Schmidt, M. Crow, and G. G. Brownlee.** 2006. Amino acid residues in the N-terminal region of the PA subunit of influenza A virus RNA polymerase play a critical role in protein stability, endonuclease activity, cap binding, and virion RNA promoter binding. J. Virol. **80:**7789–7798.
14. **He, X., et al.** 2008. Crystal structure of the polymerase PA(C)-PB1(N) complex from an avian influenza H5N1 virus. Nature **454:**1123–1126.
15. **Hodel, A. E., P. D. Gershon, X. Shi, S. M. Wang, and F. A. Quiocho.** 1997. Specific protein recognition of an mRNA cap through its alkylated base. Nat. Struct. Biol. **4:**350–354.
16. **Hu, G., P. D. Gershon, A. E. Hodel, and F. A. Quiocho.** 1999. mRNA cap recognition: dominant role of enhanced stacking interactions between methylated bases and protein aromatic side chains. Proc. Natl. Acad. Sci. U. S. A. **96:**7149–7154.
17. **Iwatsuki-Horimoto, K., et al.** 2008. Limited compatibility between the RNA polymerase components of influenza virus type A and B. Virus Res. **135:**161–165.
18. **Izaurralde, E., J. Stepinski, E. Darzynkiewicz, and I. W. Mattaj.** 1992. A cap binding protein that may mediate nuclear export of RNA polymerase II-transcribed RNAs. J. Cell Biol. **118:**1287–1295.
19. **Kawaguchi, A., T. Naito, and K. Nagata.** 2005. Involvement of influenza virus PA subunit in assembly of functional RNA polymerase complexes. J. Virol. **79:**732–744.
20. **Labadie, K., E. Dos Santos Afonso, M. A. Rameix-Welti, S. van der Werf, and N. Naffakh.** 2007. Host-range determinants on the PB2 protein of influenza A viruses control the interaction between the viral polymerase and nucleoprotein in human cells. Virology **362:**271–282.
21. **Lamb, R. A., and P. W. Choppin.** 1977. Synthesis of influenza virus polypeptides in cells resistant to alpha-amanitin: evidence for the involvement of cellular RNA polymerase II in virus replication. J. Virol. **23:**816–819.
22. **Li, C., M. Hatta, S. Watanabe, G. Neumann, and Y. Kawaoka.** 2008. Compatibility among polymerase subunit proteins is a restricting factor in reassortment between equine H7N7 and human H3N2 influenza viruses. J. Virol. **82:**11880–11888.
23. **Mazza, C., A. Segref, I. W. Mattaj, and S. Cusack.** 2002. Large-scale induced fit recognition of an m(7)GpppG cap analogue by the human nuclear cap-binding complex. EMBO J. **21:**5548–5557.
24. **Neumann, G., et al.** 1999. Generation of influenza A viruses entirely from cloned cDNAs. Proc. Natl. Acad. Sci. U. S. A. **96:**9345–9350.
25. **Neumann, G., A. Zobel, and G. Hobom.** 1994. RNA polymerase I-mediated expression of influenza viral RNA molecules. Virology **202:**477–479.
26. **Niedzwiecka, A., et al.** 2002. Biophysical studies of eIF4E cap-binding protein: recognition of mRNA 5′ cap structure and synthetic fragments of eIF4G and 4E-BP1 proteins. J. Mol. Biol. **319:**615–635.
27. **Obayashi, E., et al.** 2008. The structural basis for an essential subunit interaction in influenza virus RNA polymerase. Nature **454:**1127–1131.
28. **Ogino, T., M. Kobayashi, M. Iwama, and K. Mizumoto.** 2005. Sendai virus RNA-dependent RNA polymerase L protein catalyzes cap methylation of virus-specific mRNA. J. Biol. Chem. **280:**4429–4435.
29. **Plotch, S. J., J. Tomasz, and R. M. Krug.** 1978. Absence of detectable capping and methylating enzymes in influenza virions. J. Virol. **28:**75–83.
30. **Shimizu, K., H. Handa, S. Nakada, and K. Nagata.** 1994. Regulation of influenza virus RNA polymerase activity by cellular and viral factors. Nucleic Acids Res. **22:**5047–5053.
31. **Sugiyama, K., et al.** 2009. Structural insight into the essential PB1-PB2 subunit contact of the influenza virus RNA polymerase. EMBO J. **28:**1803–1811.
32. **Tomassini, J. E.** 1996. Expression, purification, and characterization of orthomyxovirus: influenza transcriptase. Methods Enzymol. **275:**90–99.
33. **Tomoo, K., et al.** 2002. Crystal structures of 7-methylguanosine 5′-triphosphate (m(7)GTP)- and P(1)-7-methylguanosine-P(3)-adenosine-5′,5′-triphosphate (m(7)GpppA)-bound human full-length eukaryotic initiation factor 4E: biological importance of the C-terminal flexible region. Biochem. J. **362:**539–544.
34. **Tomoo, K., et al.** 2003. Structural features of human initiation factor 4E, studied by X-ray crystal analyses and molecular dynamics simulations. J. Mol. Biol. **328:**365–383.
35. **Turan, K., et al.** 2004. Nuclear MxA proteins form a complex with influenza virus NP and inhibit the transcription of the engineered influenza virus genome. Nucleic Acids Res. **32:**643–652.
36. **Yuan, P., et al.** 2009. Crystal structure of an avian influenza polymerase PA(N) reveals an endonuclease active site. Nature **458:**909–913.

Apical Transport of Influenza A Virus Ribonucleoprotein Requires Rab11-positive Recycling Endosome

Fumitaka Momose[1]*, Tetsuya Sekimoto[1], Takashi Ohkura[1], Shuichi Jo[2], Atsushi Kawaguchi[1,2], Kyosuke Nagata[2], Yuko Morikawa[1]

1 Kitasato Institute for Life Sciences, Kitasato University, Tokyo, Japan, **2** Graduate School of Comprehensive Human Sciences, University of Tsukuba, Tsukuba, Ibaraki, Japan

Abstract

Influenza A virus RNA genome exists as eight-segmented ribonucleoprotein complexes containing viral RNA polymerase and nucleoprotein (vRNPs). Packaging of vRNPs and virus budding take place at the apical plasma membrane (APM). However, little is known about the molecular mechanisms of apical transport of newly synthesized vRNP. Transfection of fluorescent-labeled antibody and subsequent live cell imaging revealed that punctate vRNP signals moved along microtubules rapidly but intermittently in both directions, suggestive of vesicle trafficking. Using a series of Rab family protein, we demonstrated that progeny vRNP localized to recycling endosome (RE) in an active/GTP-bound Rab11-dependent manner. The vRNP interacted with Rab11 through viral RNA polymerase. The localization of vRNP to RE and subsequent accumulation to the APM were impaired by overexpression of Rab binding domains (RBD) of Rab11 family interacting proteins (Rab11-FIPs). Similarly, no APM accumulation was observed by overexpression of class II Rab11-FIP mutants lacking RBD. These results suggest that the progeny vRNP makes use of Rab11-dependent RE machinery for APM trafficking.

Citation: Momose F, Sekimoto T, Ohkura T, Jo S, Kawaguchi A, et al. (2011) Apical Transport of Influenza A Virus Ribonucleoprotein Requires Rab11-positive Recycling Endosome. PLoS ONE 6(6): e21123. doi:10.1371/journal.pone.0021123

Editor: Jean-Luc E.P.H. Darlix, Institut National de la Santé et de la Recherche Médicale, France

Received March 19, 2011; **Accepted** May 19, 2011; **Published** June 22, 2011

Funding: This work was supported in part by a grant-in-aid from the Ministry of Education, Culture, Sports, Science, and Technology of Japan (FM KN YM), Research Fellowship of the Japanese Society for the Promotion of Science (JSPS) (AK), and by a Kitasato University Research Grant for Young Researchers (FM). The funders had no role in study design, data collection and analysis, decision to publish, or preparation of the manuscript.

Competing Interests: The authors have declared that no competing interests exist.

* E-mail: fmomose@lisci.kitasato-u.ac.jp

Introduction

The viral genomes do not exist alone but form nucleoprotein complexes in which DNA/RNA genome is complexed with viral basic proteins, e.g., nucleocapsid protein for retrovirus [1] and core protein VII for adenovirus [2,3]. In the case of influenza A virus, a member of *Orthomyxoviridae*, a virion contains eight distinct segments of viral/virion ribonucleoprotein complexes (vRNPs) and each vRNP segment consists of a single-stranded negative-sense virion RNA (vRNA), viral RNA-dependent RNA polymerase (heterotrimer of PB2, PB1, and PA subunits), and nucleoprotein (NP) [4]. Both 5′ and 3′ termini of vRNA segment form a partially complementary double-stranded structure called "panhandle" [5,6] and function as promoter and replication origin for viral RNA synthesis. The viral RNA polymerase primarily binds to the panhandle region, whereas NP binds to the single-stranded region [7,8,9,10]. During viral genome replication, complementary RNA (cRNA) segments are synthesized from vRNA segments and progeny vRNAs are further amplified from the cRNA segments. Although both cRNA and progeny vRNA form viral RNP complexes, it has been shown that cRNP only localizes in the nucleus [11,12].

Trafficking of viral genome-nucleoprotein complex from the cell surface to sites of viral genome replication involves cellular trafficking machineries [13,14]. Some viruses, e.g., HIV-1 and herpes simplex virus (HSV), fuse with the plasma membrane and their nucleoprotein complexes ride on "tracks" such as actin filaments and microtubules [15,16]. Other viruses, e.g., Semliki Forest virus, adenovirus, and influenza virus, taken up by endocytosis [17,18,19,20], might be transported on the cytoskeletal tracks in the cytoplasm. In the case of influenza virus, trafficking of endocytosed virions to the perinuclear region has been visualized by live cell imaging [21]. It is well known that endocytosed influenza virus is uncoated at low pH endosomes and vRNP segments are relocated into the nucleus where replication of influenza virus genome occurs [22].

Newly synthesized nucleoprotein forms a complexes with viral genome and the complex is transported to sites of genome packaging/virion budding: the apical plasma membrane (APM) of polarized epithelial cells for influenza virus and respiratory syncytial virus (RSV) [23,24]; the basolateral plasma membrane for vesicular stomatitis virus [23,25]; intracellular membranes for herpes viruses [26]. Like viral entry, these viral egress pathways depend on cytoskeletons, transport vesicles, and/or motor proteins [27]. To identify such transport pathways utilized for incoming and outgoing viruses, a number of organelle marker proteins, e.g., EEA1, mannose 6-phosphate receptors, LAMP1, and small GTPase Rab family proteins are used [28,29]. Progeny viruses were finally released from cells by cell lysis or membrane budding followed by pinching-off. The endosomal sorting complex required for transport (ESCRT) machinery, especially ESCRT-III and VPS4 were often used for release of some viruses such as

retroviruses [30,31]. However, other viruses require additional release machinery (e.g., prototype foamy virus and parainfluenza virus 5) [32,33,34] or do not require the ESCRT machinery (e.g., RSV and influenza virus) [35,36,37]. It has been reported that release of RSV is independent of ESCRT machinery but controlled by Rab11 family interacting protein 2 (Rab11-FIP2), an effector protein of Rab11 [35]. Similarly, influenza virus particle budding and filamentous viral formation are controlled by the Rab11 system including a related factor(s) such as Rab11-FIP3 [38].

To elucidate these trafficking pathways for outgoing viruses, live cell imaging has been employed and revealed that microtubules are tracks for egress of vaccinia virus [39,40,41]. Single-stranded RNA virus genomes (e.g., poliovirus and RSV) have also been visualized with fluorescent antisense nucleotide probes called molecular beacon in living cells [42,43]. However, such viral genomes are complexed with viral nucleoproteins, which are the essence of viral infectivity, but nevertheless is poorly delineated because of a lack of specific detection system. We obtained anti-NP monoclonal antibody (mAb61A5) that preferentially bound to influenza viral RNP complexes rather than free NP and found that progeny viral RNP complexes distributed as punctate signals and concentrated at the microtubule organizing center (MTOC) in fixed cells [44]. Fluorescence *in situ* hybridization (FISH) assays confirmed that the punctate RNP signals contained negative-sense viral RNA [45]. Here, we report that progeny vRNPs of influenza virus primarily target to the small GTPase Rab11-positive recycling endosome (RE), also known as endocytic recycling compartment (ERC), through interaction between an active/GTP-bound Rab11 molecule(s) and a heterotrimeric viral RNA-dependent RNA polymerase of vRNP. Our data also indicate that the targeting to RE is required for the cytoplasmic trafficking of vRNP to the APM along microtubules and subsequent virion production. Based on our data and others, we propose a model for a higher-order assembly of vRNP segments toward virion packaging.

Results

Live cell imaging of progeny vRNP in the cytoplasm

Our previous studies with paraformaldehyde-fixed cells found the potential of anti-NP mAb61A5 for detection of the vRNPs in the cytoplasm of influenza virus infected cells [44,45]. Anti-NP mAb61A5 preferentially bound to influenza viral RNP complexes and immunostaining using this antibody showed punctate NP antigens in the cytoplasm after 4 hours postinfection (hpi). Further FISH analysis revealed that the punctate NP antigen contains viral genome RNAs. These punctate signals of vRNPs were localized along the microtubules and later accumulated at the APM. Depolymerization of microtubules by nocodazole dispersed the punctate vRNP signals in the cytoplasm, suggesting microtubule-dependent transport of progeny vRNPs.

To understand dynamic events of progeny vRNP, here we carried out live cell imaging of vRNP signals (Figure 1A). To this end, fluorescent-labeled mAb61A5 was introduced into infected cells with protein transfection reagents. Dual-color imaging of mAb61A5 (Figure 1A, red) and non-specific control antibody (Figure 1A, green) eliminated pseudo-positive signals, likely corresponding to aggregates of antibodies and non-specifically endocytosed antibodies upon liposome-mediated transfection (Figure 1A, arrowheads, yellow in merged image) and allowed us to detect true outgoing vRNP signals (red alone in merged image). Live cell imaging revealed that the vRNP signals moved rapidly but intermittently in both forward and backward directions (Figure 1A and Video S1). We defined one motile event as a single unidirectional movement (see Materials and Methods). Tracking of vRNP signals showed that 72% of mean velocities (V_{mean}) of individual motile events were ranged from 0.75 to 2.00 μm/s and the mean overall V_{mean} was 1.45 μm/s (Figure 1B and Table S7). This mean velocity is likely to correspond to a microtubule- and motor protein-dependent vesicular transport, since it has been reported that KIF1A particles moved in axons anterogradely at 1.00±0.61 μm/s and sometimes retrogradely at 0.72±0.27 μm/s [46], (see the discussion). Some of the maximum velocities (V_{max}) observed in individual events reached over 5.00 μm/s (Figure 1C). Mean of migration lengths of individual events was 2.68 μm and the maximum length reached 7.48 μm (Video S1 and Table S7, trajectory No. 5, during 14.00 to 18.25 s). Mock-infected MDCK cells with heat-inactivated virus did not show any vRNP-specific signals but only pseudo-positive signals (Video S2, left half).

To analyze whether vRNP signals move along microtubules, we established an AcGFP-α-tubulin expressing MDCK cell line (MDCK-Tub) and carried out dual-color imaging (Figure 2). Progeny vRNP signals localized to (Figure 2, panels A and B) and moved along microtubules (Figure 2C and Video S3). A vRNP signal (Figure 2D, arrowheads) often moved intermittently: (i) pausing (0.0 to 33.6 s), (ii) moving (event 1, 33.6 to 36.6 s, duration of 3.0 s), (iii) pausing again (36.6 to 38.4 s), and (iv) moving again (event 2, 38.4 to 41.4 s, duration of 3.0 s). These observations indicated that progeny vRNPs are transported through the microtubule-dependent trafficking machinery.

Progeny vRNPs are colocalized with Rab11-positive compartments in the cytoplasm

We have previously reported that the vRNP signals were colocalized with microtubules and concentrated at the MTOC [44]. Given the fact that cytoplasmic vesicles are often accumulated at the MTOC and are transported on microtubules [14], our data suggest that the vRNPs were able to be transported on vesicles. Indeed, the behavior of vRNP signals we observed by live cell imaging (Figures 1 and 2, Videos S1 and S3) resembled that of Rab10, small GTPase protein involved in vesicle trafficking [47]. Based on these hypotheses, we carried out identification of cytoplasmic compartments involved in vRNP trafficking by immunofluorescence microscopy. We constructed 20 distinct classes of Rab proteins as markers for transport vesicles, all of which were tagged with AcGFP (Table S1, except for Rab11B). Each of Rab family proteins is implicated in distinct vesicle trafficking [28,29]. We assessed the colocalization with vRNPs by confocal microscopy: AcGFP-Rab11A was almost completely, and AcGFP-Rab25 and -Rab17 were partially colocalized with vRNP signals (Figure 3, panels A, B, and C, respectively). The others we tested did not show significant colocalizations with vRNP signals (data not shown). Since Rab11A [48,49,50], Rab25 [51,52], and Rab17 [53,54] are known as marker proteins of RE, our results suggested that the progeny vRNP segments were transported via RE.

Although these three Rab proteins participate in RE trafficking [28,29], their precise distributions may differ from each other. We coexpressed either FLAG-Rab25 or FLAG-Rab17 with AcGFP-Rab11A in MDCK cells and observed their localizations (Figure 3D). The majority of FLAG-Rab25 was colocalized with AcGFP-Rab11A (Figure 3D, upper images), whereas FLAG-Rab17 was rarely colocalized with AcGFP-Rab11A except for the perinuclear region, which may correspond to the pericentriolar ERC/RE (Figure 3D, lower images). From these results, we

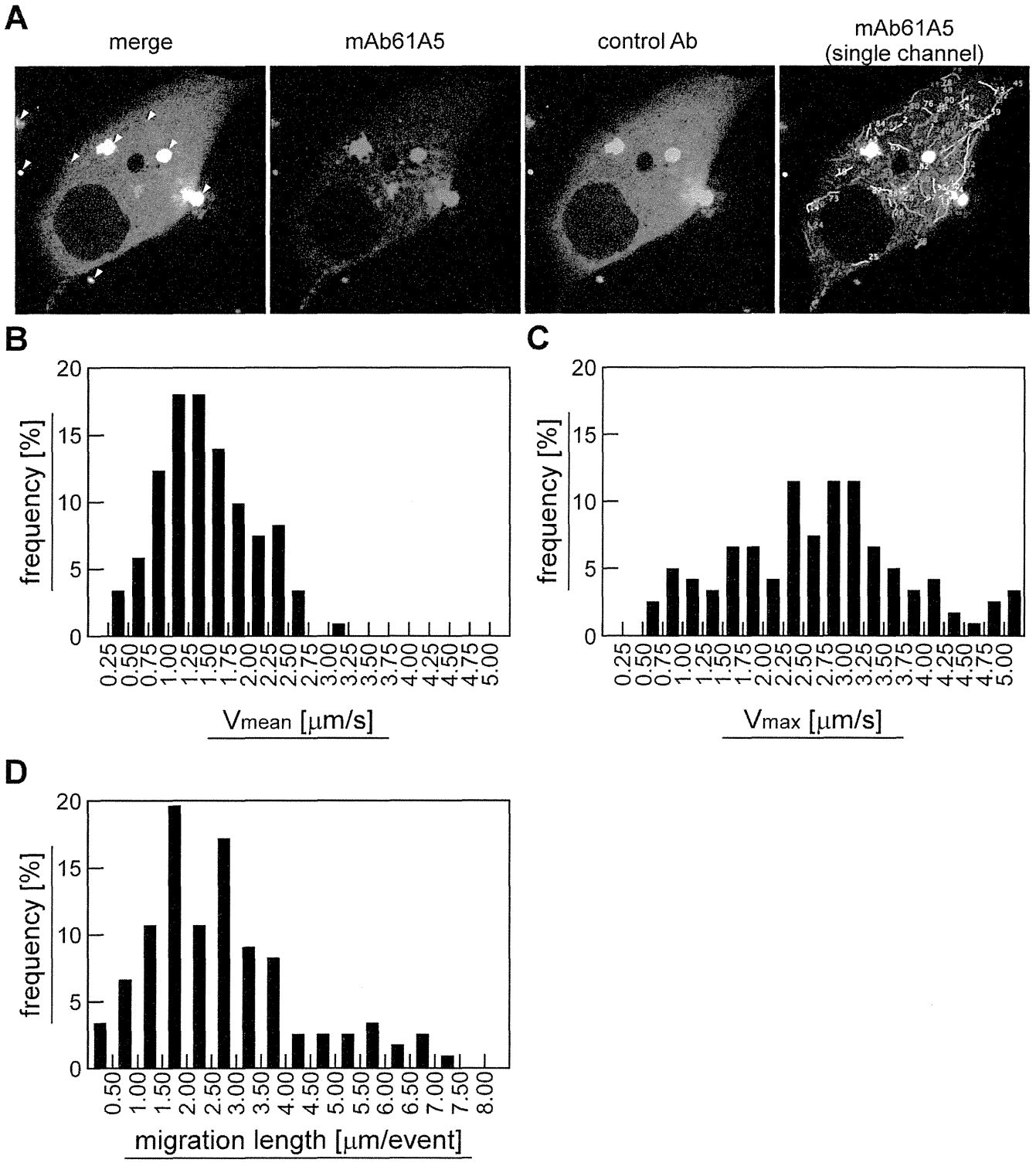

Figure 1. Live cell imaging of cytoplasmic vRNPs in infected MDCK cells. (**A**) For live cell imaging, AF568-conjugated anti-NP mAb61A5 (red, mAb61A5) and AF488-conjugated non-specific mouse immunoglobulin (green, control Ab) were cotransfected to infected MDCK cells. Sequential images were acquired by the dual-color protocol and subsequently by the single-color protocol for kinetic analysis. Images were processed and analyzed by using ImageJ software and MTrackJ plugin (Video S1). A representative frame of the movie was shown (left 3 images). Pseudo-positive signals appeared in yellow in merged image (most left image, arrowheads). An example of signal tracking was shown as trajectories (most right image, mAb61A5 single channel). (**B** and **C**) Velocity distribution of vRNP signals. Mean and maximum velocities (V_{mean} and V_{max}, respectively) of individual motile events were calculated and shown as histograms (Table S7, total 123 motile events derived from 75 trajectories). (**D**) Distribution of migration lengths. The migration lengths of individual motile events were shown as a histogram.
doi:10.1371/journal.pone.0021123.g001

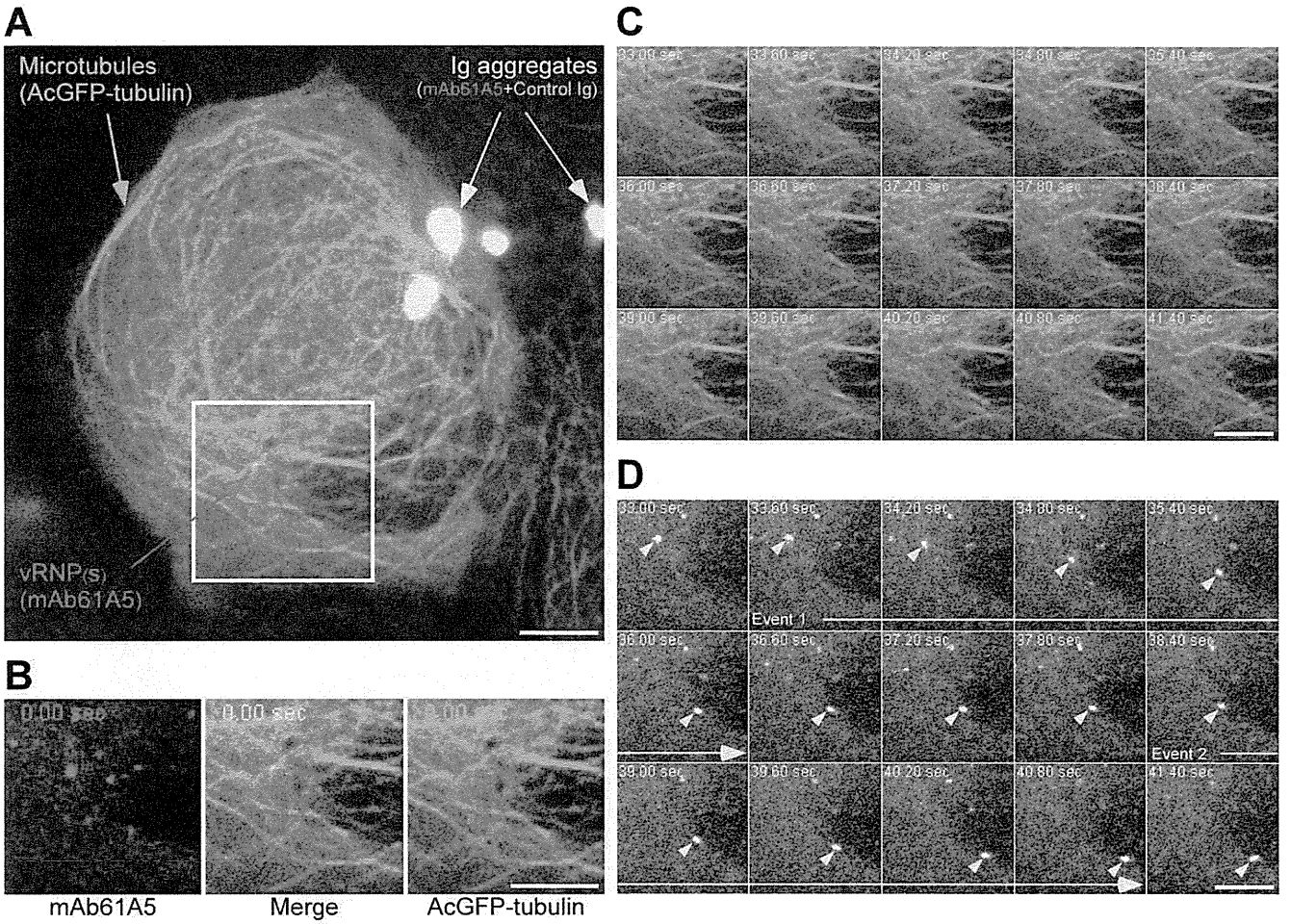

Figure 2. Live cell imaging of cytoplasmic vRNPs along microtubules. (**A**) Live cell imaging was carried out using MDCK cells expressing AcGFP-α-tubulin. Pseudo-positive signals (yellow), the microtubule networks (green), and vRNPs (red) were indicated as arrows. (**B**) Cropped and each color-split image of the indicated area (white box in panel A). Sequential images were shown in Video S3. (**C** and **D**) Time-split images of the merged images and the mAb61A5 channel images in the cropped area, respectively. Elapsed time from the first acquisition was indicated on each image. A vRNP signal (arrowheads in D) moved (event 1, 33.6 to 36.0 s), paused (36.0 to 38.4 s), and moved again (event 2, 38.4 to 40.8 s). Scale bars = 5 μm.
doi:10.1371/journal.pone.0021123.g002

reasoned that progeny vRNPs might target and accumulate to the Rab11-positive RE in the cytoplasm.

We verified the colocalization of cytoplasmic vRNP with endogenous Rab11. Confocal imaging revealed that vRNPs colocalized with endogenous Rab11 at the cell periphery of MDCK cells at 7 h postinfection (hpi) (Figure 3E). The fluorescent image of xz plane reconstituted from the image stack showed that, at this time point, the majority of progeny vRNPs were colocalized with Rab11 and both were accumulated at the upper cell surface (Figure 3F), although a fraction of endogenous Rab11 remained at the perinuclear region.

Active/GTP-bound Rab11 is required for localization of progeny vRNP to RE

The small GTPase Rab family protein is activated upon GTP binding and is inactivated by GTP hydrolysis [55,56]. The single-point mutations around the GTPase active site, i.e., substitutions of the serine residue at amino acid position 25 to an asparagine residue (S25N) or the glutamine residue at amino acid position 70 to a leucine residue (Q70L), have been shown to stabilize the Rab11A protein in GDP- or GTP-bound states [49]. To test whether expression of GDP/GTP-locked Rab11 affects the localization of vRNP to RE, we constructed dominant negative (designated DN, S25N substitution) and constitutively active (designated CA, Q70L substitution) mutants of FLAG-Rab11A and expressed in MDCK cells. Transient expression of CA Rab11A did not alter the localization of progeny vRNP signals to RE (Figure 4A, right images) but, in contrast, expression of the DN Rab11A markedly impaired the localization to RE, showing that vRNP was diffusely distributed throughout the cytoplasm (Figure 4A, center images). Essentially similar results were observed when Rab11B and its mutants were used (data not shown). These results indicate that progeny vRNP targeting and/or localization to RE require active/GTP-bound Rab11.

Next, we examined their impacts on viral replication (Figure 4B). Influenza virus was infected to MDCK cell lines in which wild type (WT), DN mutant, and CA mutant of FLAG-Rab11A were constitutively expressed (MDCK-F11A-WT, -DN, and -CA, respectively), and infectious progeny viruses were titrated by plaque assays. No significant differences in the kinetics of infectious virus production were observed between MDCK-F11A-CA and -WT cells and even with MDCK cells containing the empty vector (MDCK-Neo). However, viral production in MDCK-F11A-DN cell line was severely impaired with a 99.0–99.9% reduction at 24

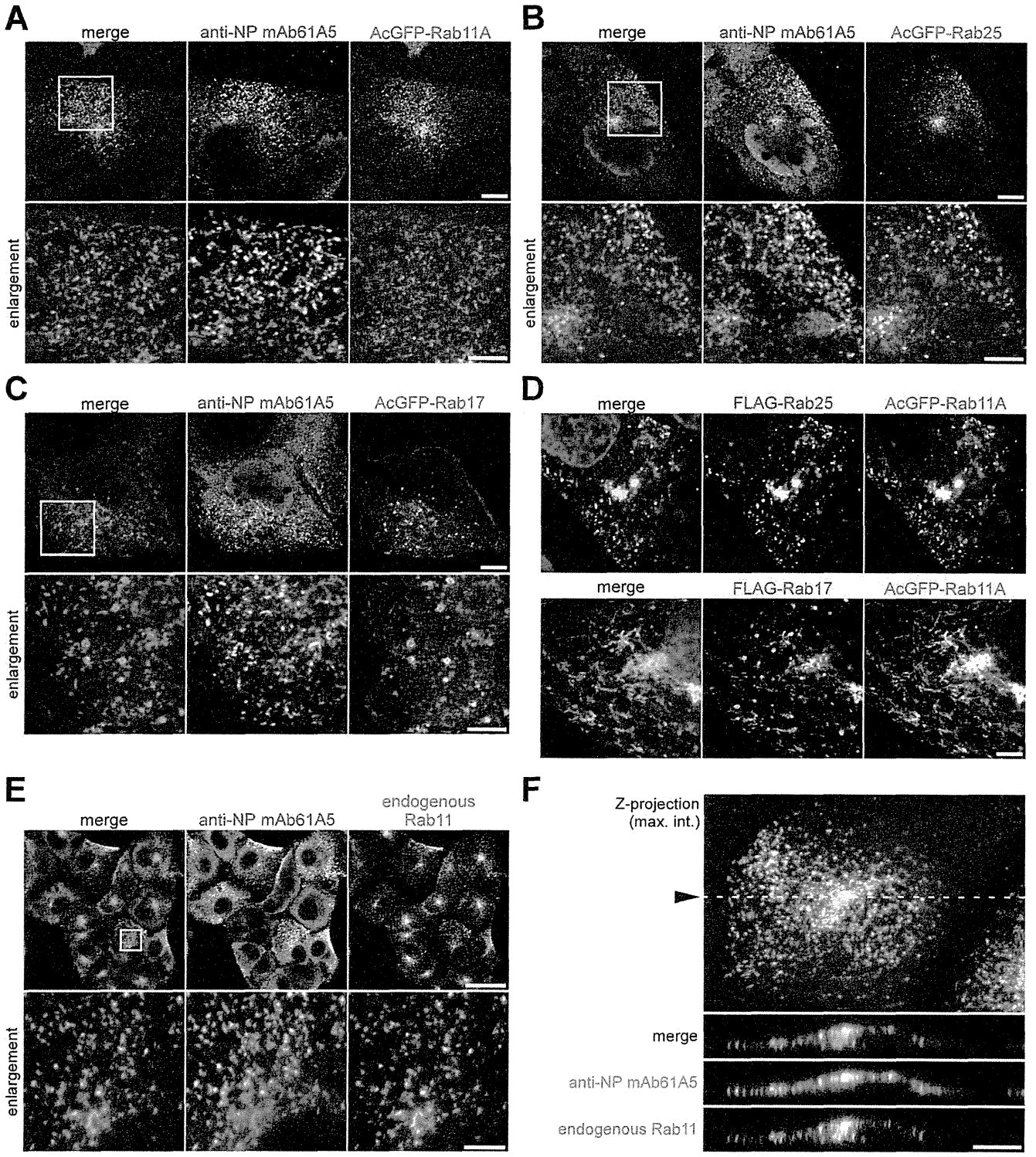

Figure 3. Colocalization of punctate vRNP signals with Rab11. (**A–C**) Localizations of cytoplasmic vRNPs and transiently expressed human Rab proteins. Influenza A virus was infected to MDCK cells transiently expressing AcGFP-tagged human Rab11A, Rab25, and Rab17 (panels A–C, respectively). At 7 hpi, vRNPs were immunostained with mAb61A5 (center image in each set) and visualized by confocal microscopy with AcGFP-Rab proteins (right images). Enlarged images of indicated areas (white boxed) were also shown (lower images). Scale bars are 10 and 5 μm (upper and lower images, respectively). (**D**) Localizations of transiently expressed human Rab11A, Rab25, and Rab17. FLAG-Rab25 (upper) and FLAG-Rab17 (lower) (center images) were coexpressed with AcGFP-Rab11A (right images) in MDCK cells. Nuclei were stained with DAPI (blue, left images). Scale bar is 5 μm. (**E** and **F**) Colocalization of vRNP with endogenous Rab11. Progeny vRNPs were similarly stained with mAb61A5. Endogenous canine Rab11 (right images) was visualized with rabbit anti-Rab11 polyclonal antibody. (E) XY presentation. Scale bars are 40 and 5 μm (upper and lower images, respectively). (F) XZ presentation. Z-stacks of confocal images were acquired at 0.5 μm z-axis interval. Z-projection of maximum intensities (top image) and reconstitution of a xz plane (lower 3 images) were processed by using ImageJ software. Dotted line indicates the position of the reconstituted xz plane. Scale bar is 10 μm.
doi:10.1371/journal.pone.0021123.g003

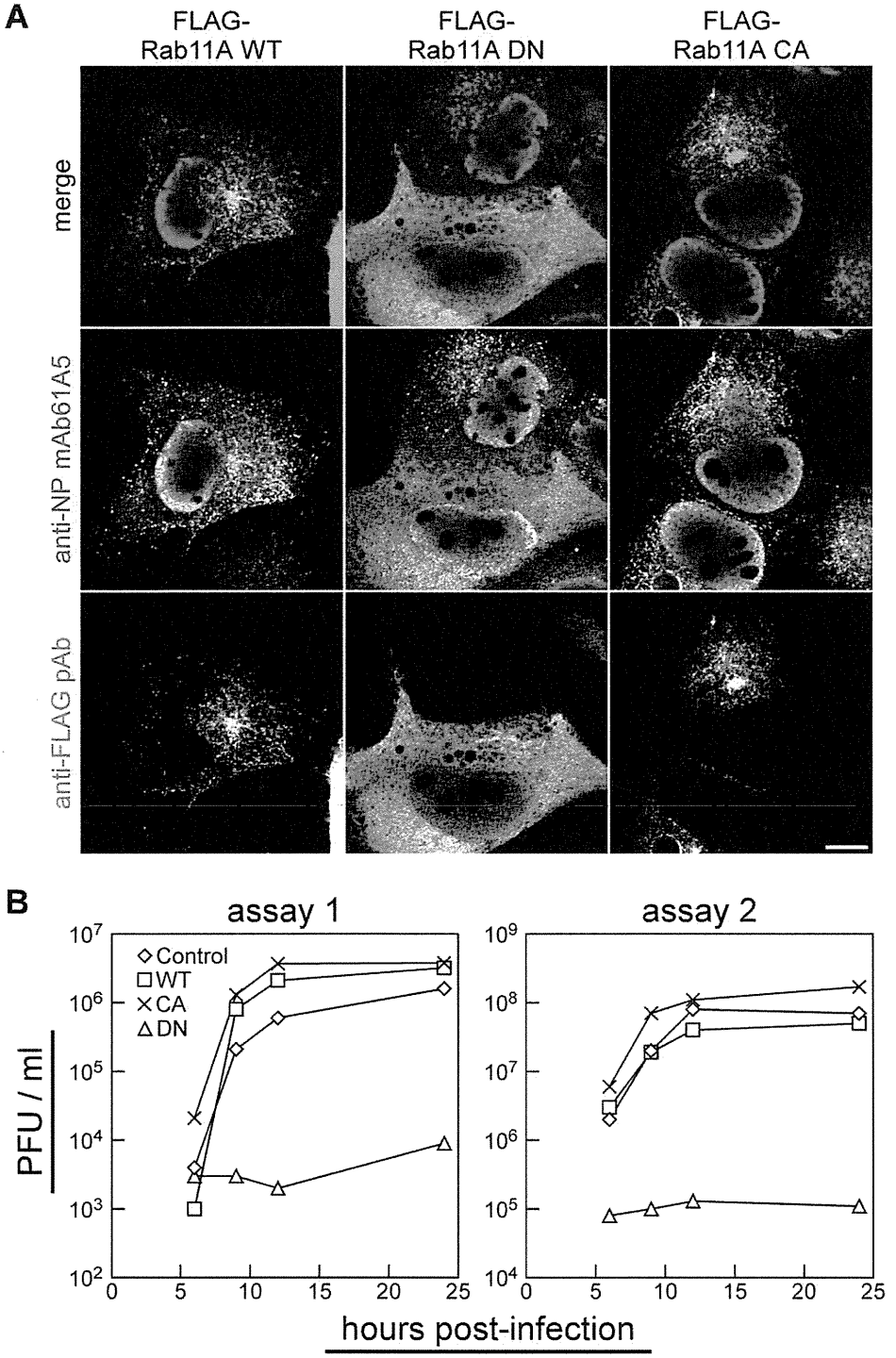

Figure 4. Localization of progeny vRNPs to RE in active/GTP-bound Rab11 dependent manner. (**A**) Alteration of vRNP localization by transient expression of dominant negative Rab11 mutant. Influenza A virus was infected to MDCK cells transiently expressing the wild type (WT, left images), dominant negative (DN, center images), and constitutively active (CA, right images) forms of FLAG-tagged human Rab11A. At 7 hpi, vRNPs (middle images) and FLAG-Rab proteins (bottom images) were immunostained using mAb61A5 and rabbit anti-FLAG polyclonal antibody (pAb) and observed by confocal microscopy. Scale bar is 10 μm. (**B**) Production of infectious progeny viruses from infected MDCK cells constitutively expressing human Rab11A and its mutants. Culture supernatants of MDCK cells infected with PR8 strain at moi = 1 to 3 were temporally harvested and titers of infectious viruses were measured and indicated as plaque forming unit (pfu)/ml. Single-round infection experiments were carried out using different lots of viral inoculum in independent experiments.
doi:10.1371/journal.pone.0021123.g004